An improved auxin-inducible degron system preserves native protein levels and enables rapid and specific protein depletion

Kizhakke Mattada Sathyan[a], Brian D. McKenna[a], Warren Anderson[b], Fabiana M. Duarte[d], Leighton J. Core[e], and Michael J. Guertin[a,b,c,] ✉

[a]Biochemistry and Molecular Genetics Department, University of Virginia, Charlottesville, Virginia, United States of America
[b]Center for Public Health Genomics, University of Virginia, Charlottesville, Virginia, United States of America
[c]Cancer Center, University of Virginia, Charlottesville, Virginia, United States of America
[d]Department of Stem Cell and Regenerative Biology, Harvard University, Cambridge, Massachusetts, United States of America
[e]Department of Molecular and Cell Biology, University of Connecticut, Storrs, Connecticut, United States of America

Rapid perturbation of protein function permits the ability to define primary molecular responses while avoiding downstream cumulative effects of protein dysregulation. The auxin-inducible degron (AID) system was developed as a tool to achieve rapid and inducible protein degradation in non-plant systems. However, tagging proteins at their endogenous loci results in chronic, auxin-independent degradation by the proteasome. To correct this deficiency, we expressed the Auxin Response Transcription Factor (ARF) in an improved inducible degron system. ARF is absent from previously engineered AID systems, but ARF is a critical component of native auxin signaling. In plants, ARF directly interacts with AID in the absence of auxin and we found that expression of the ARF Phox and Bem1 (PB1) domain suppresses constitutive degradation of AID-tagged proteins. Moreover, the rate of auxin-induced AID degradation is substantially faster in the ARF-AID system. To test the ARF-AID system in a quantitative and sensitive manner, we measured genome-wide changes in nascent transcription after rapidly depleting the ZNF143 transcription factor. Transcriptional profiling indicates that ZNF143 activates transcription in *cis* and ZNF143 regulates promoter-proximal paused RNA Polymerase density. Rapidly inducible degradation systems that preserve the target protein's native expression levels and patterns will revolutionize the study of biological systems by enabling specific and temporally defined protein dysregulation.

Auxin Inducible Degron | Auxin Response Factor | ZNF143 | Transcription Factors | RNA Polymerase Pausing

Correspondence: ***guertin@virginia.edu***

Introduction

The function of proteins can be studied in cells using RNAi depletion, loss-of-function mutants, temperature sensitive mutations, small molecule inhibitors, CRISPR interference, or nucleic acid aptamers. The two greatest limitations of these methods are 1) the chronic nature of permanently disrupting function and 2) the limited availability and specificity of inhibitor molecules. Inducible degradation methods, such as auxin-inducible degron (AID) (1) or degradation tag (dTAG) systems (2), can overcome these limitations. Rapidly regulated systems and inhibitors permit measurements of primary changes in molecular, cellular, and organismal phenotypes and subsequent tracking of the cascade that accompanies immediate protein dysregulation. Gene editing techniques now permit endogenous tagging of genes, which should preserve the target gene's expression levels and patterns. Endogenous fusion of target genes with rapidly inducible degradation tags have the potential to revolutionize the way we study biological systems by providing specific and temporally defined perturbation techniques for any protein of interest.

Auxin is a plant hormone that regulates various aspects of plant growth and development. In plants, auxin signaling triggers a rapid switch between transcriptional repression and transcriptional activation (3–5) (Figure S1). There are three key components in this signal transduction system: 1) transport inhibitor response 1 (TIR1), a subunit of a ubiquitin ligase complex that binds to the target substrate; 2) the auxin response transcription factors (ARF), which directly regulate gene expression; and 3) auxin/indole-3-acetic acid (Aux/IAA) proteins, which are destabilized in the presence of auxin-mediated ubiquitination. In the absence of auxin, the domains III&IV of Aux/IAA family of proteins form heterodimeric complexes with the Phox and Bem1 (PB1) domain of ARF proteins (6, 7). Domain I of Aux/IAA interacts with a plant-specific transcriptional co-repressor, Topless (TPL) (8). The repressive function of TPL dominates relative to the activation function of ARF transcription factors (9). In the presence of auxin, TIR1 interacts with domain II of Aux/IAA to facilitate ubiquitination and degradation of Aux/IAA (10, 11), which liberates ARFs to regulate transcription. This auxin-inducible degron system was engineered to function outside plant cells (1).

Although the AID system has been widely adopted to degrade tagged proteins of interest, recent studies report auxin-independent depletion of endogenously tagged proteins (12–14). For instance, tagging the centromeric histone chaperone, HJURP, results in depletion of more than 90% of protein in the absence of auxin in human cell lines (14). Chronic depletion has also been reported in chicken cells (13) and in yeast cells (12), suggesting that auxin-independent depletion may be a systemic problem when tagging endogenous genes. The extent of factor-dependent depletion is often impossible to evaluate because many studies do not directly compare protein levels in the progenitor and tagged cell lines (15–17). Neither defining a minimal degradation domain of AID nor employing an inducible TIR1 system have overcome this deficiency (12, 18, 19). In yeast, auxin-independent depletion of the AID-tagged factors is dependent on cellular TIR1 concentration, suggesting that depletion is due to ubiquitin-mediated degradation (18).

Herein, we show that AID-tagging of endogenous genes commonly results in auxin-independent and chronic depletion by proteasome-mediated protein degradation. We found that co-expressing the PB1 domain of ARF improved the robustness of the AID system by rescuing auxin-independent degradation and increasing the rate of auxin-induced degradation. Our control experiments also revealed that auxin treatment alone results in the activation of the Aryl Hydrocarbon Receptor (AHR) transcription factor and regulation of AHR target genes. Excluding AHR-responsive genes from downstream differential expression analyses is critical when investigating the activity of AID-tagged transcriptional regulators. Collectively, these improvements enhance the robustness, sensitivity, and specificity of the AID system. We applied ARF-rescue, AID-mediated, rapid degron depletion to the transcription factor ZNF143 to identify the primary ZNF143 response genes and to define a functional role of ZNF143 in transcriptional regulation.

Results

Endogenous auxin-inducible degron tagging results in chronic target protein depletion.

In non-plant systems, the auxin-mediated degradation system requires the presence of exogenously expressed TIR1 (1). We generated an HEK293T cell line with the TIR1 gene stably integrated into the AAVS1 locus (20, 21) (Figure S2). We independently tagged all copies of either ZNF143, TEAD4, and p53 in these progenitor HEK293T-TIR1 cells (Figure 1A). In the absence of auxin, tagging the factors resulted in depletion of the proteins to levels that range from between <3%-15% of endogenous levels, as measured by quantitative Western blots (Figure 1B,C,&D). To determine whether chronic depletion is unique to HEK293T cells, we generated an MCF-7 cell line with TIR1 incorporated heterozygously into the AAVS1 locus and tagged all copies of ZNF143, which also resulted in auxin-independent ZNF143 depletion (Figure 1E). Next, we characterized a previously published AID-tagged CENP-I colorectal epithelial DLD-1 cell line (15). CENP-I is also modestly depleted (Figure 1F). The modest degree of CENP-I depletion may be because CENP-I is an essential protein and a minimal abundance of CENP-I is necessary for cell line viability. Basal depletion of these factors in three distinct cell lines confirms the generality of auxin-independent depletion of endogenously tagged proteins.

Proteasome mediated degradation drives auxin-independent depletion of proteins.

We next sought to investigate the mechanism by which AID-tagged proteins are depleted by focusing on AID-tagged ZNF143. We performed nascent RNA sequencing (22–24) in the progenitor HEK293T-TIR1 cells and the ZNF143-AID cells. Nascent ZNF143 transcript levels remain unchanged (1.08-fold increase, FDR = 0.27) in the AID-tagged ZNF143 cell line (Figure 2A). Because the auxin-inducible system is dependent upon the proteasome and AID can interact with TIR1 in the absence of auxin (10, 25–27), we hypothesized that low protein abundance may be mediated by an auxin-independent interaction with TIR1, ubiquitination, and subsequent proteasome-mediated degradation. We treated ZNF143-AID cells with the proteasome inhibitor MG132 and observed a modest increase in ZNF143 levels after 4.5 hours (Figure S3A). TIR1 depletion (Figure S3B) also results in higher ZNF143 levels (Figure S3C). These results indicate that chronic, auxin-independent depletion of AID-tagged proteins is TIR1-mediated and due to proteasomal degradation (Figure S3D).

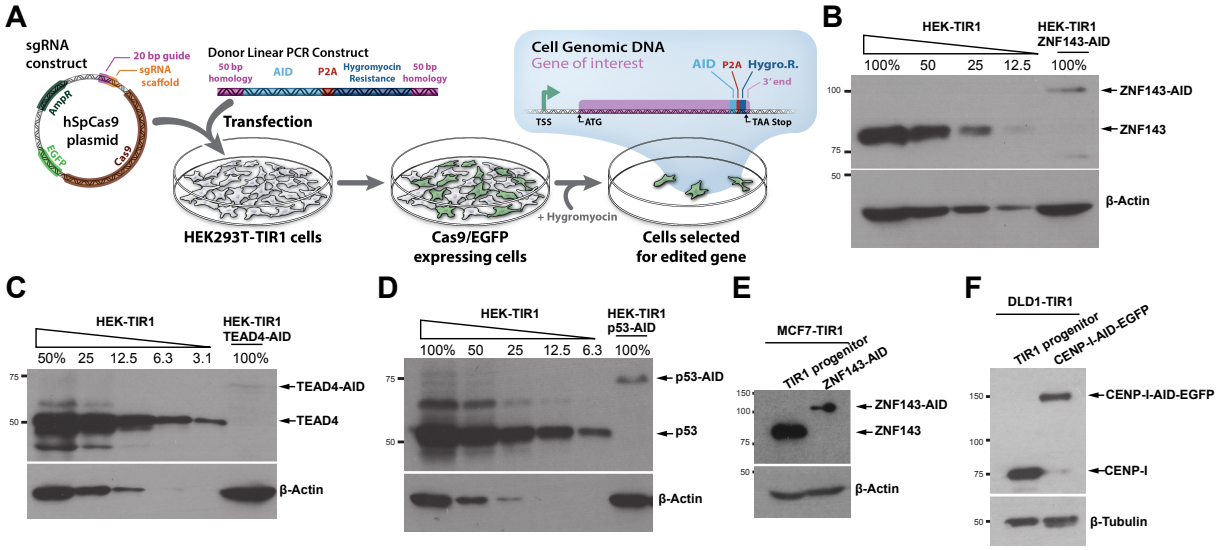

Fig. 1. Endogenous tagging of genes with AID results in auxin-independent protein depletion. A) Genes of interest were targeted by cotransfecting sgRNAs (Table 2) targeting the 3′ end of the coding sequence with a homology-directed repair donor construct. The donor construct contained the AID domain fused to a hygromycin resistance marker; an intervening porcine teschovirus-1 2A (P2A) site liberates the hygromycin resistance marker during protein translation. This construct was flanked by 50 base pair homology regions that correspond to the sequences flanking the sgRNA recognition sequence and Cas9 cleavage site. B,C,&D) We quantified AID-tagged protein abundance with quantitative Western blots and a dilution of the progenitor cell line for the standard curve. Endogenous homozygous tagging of ZNF143 (B), TEAD4 (C), and p53 (D) in HEK293T cells results in auxin-independent chronic protein depletion. MCF-7 (E) and DLD-1 (F) cell lines also exhibit depletion of endogenously tagged ZNF143 (E) and CENP-I (F).

Auxin Response Factor rescues auxin-independent proteasomal degradation.

TIR1 and AID proteins can directly interact in the absence of auxin *in vitro* (25–27). However, degradation is tightly and robustly regulated in plants (28) (Figure S1). We proposed that expression of an ARF protein, which is an AID-interaction partner, may confer protection of the tagged protein from auxin-independent ubiquitination and degradation. To test this hypothesis, we supplemented the engineered AID system by expressing the AID-interacting PB1 domain of ARF. We reconstituted the system by expressing the PB1 domain of *Oryza sativa* ARF16 and ARF25, based on yeast two-hybrid experiments that quantified interaction of these ARFs with IAA proteins (29). Moreover, ARF16 and ARF25 harbor conserved charged residues, corresponding to K944, D994, and D998 of ARF16 (30), at critical positions within the ARF/IAA binding interface (31, 32). Transfection of either eGFP-ARF25-MR-PB1 or eGFP-ARF16-PB1 stabilizes TEAD4-AID, with ARF16 promoting a higher degree of TEAD4 stability (Figure S4A&B). These results prompted us to generate HEK293T-TIR1-ZNF143-AID cells with stable genetic integration and expression of ARF16-PB1. This strategy restored ZNF143 levels to over 50% of untagged levels (Figure 2B and Figure S4C&D). Similarly, we found that genetic integration and expression of eGFP-ARF16-PB1 stabilized endogenously tagged TEAD4-AID (Figure 2C). In contrast, stable expression of eGFP-ARF16-PB1 did not alter ZNF143, TEAD4, or p53 protein levels in HEK293T or HEK293T-TIR1 cells (Figure S4E).

Transcriptional output is a quantitative measure of ARF-mediated functional rescue of ZNF143. We performed nascent RNA transcriptional profiling (22) with the three successive genetically modified HEK293T cells: progenitor TIR1 cells, chronic ZNF143-depleted AID-tagged cells, and ARF-rescued ZNF143-AID cells. Chronic ZNF143 depletion resulted in activation of 1188 genes and repression of 774 genes at a false discovery rate (FDR) of 0.001 (Figure 2A). Next, we analyzed the raw changes in expression upon ARF rescue to determine whether rescuing ZNF143 stability can functionally rescue gene expression profiles. Of the 1188 activated genes upon chronic ZNF143 depletion, 899 (76%) decrease their expression upon ARF rescue (Figure 2D). Of the 774 chronically repressed genes, 561 (72%) increase their expression upon ARF rescue (Figure 2D). These changes are consistent with a functional rescue of gene expression upon ARF rescue of ZNF143 stability.

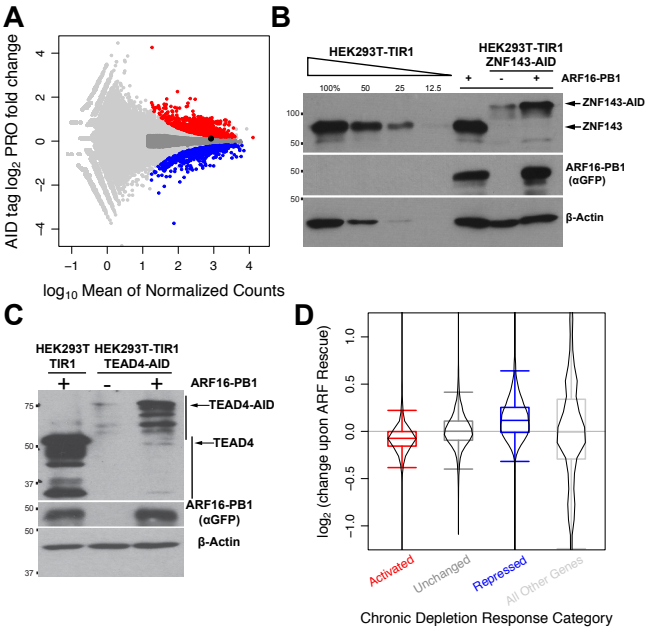

Fig. 2. Expressing the PB1 domain of ARF rescues the proteasome-dependent chronic depletion of AID-tagged proteins. A) Red genes are activated upon chronic ZNF143 depletion, blue genes are repressed, dark grey genes are confidently unchanged and expressed at comparable levels to changed genes, and light grey points represent all other genes. ZNF143 (black point) expression is unaffected. B) Stable expression of ARF-PB1 domain in HEK293T-TIR1 cells did not change the protein levels of ZNF143 (lane 5), but increased the stability of ZNF143-AID (lane 7). C) TEAD4 levels also increase upon ARF16 expression. D) Genes that are activated upon chronic ZNF143 depletion in panel A are, on average, repressed upon ARF rescue and genes that are repressed upon chronic depletion are activated upon ARF rescue.

Auxin Response Factor rescue mediates rapid auxin-inducible degradation.

We treated ZNF143-AID and TEAD4-AID cells with 500 μM auxin to determine how the ARF16 rescue affects inducible depletion. Auxin treatment induces degradation of both ZNF143-AID and TEAD4-AID in a time dependent manner (Figure 3A&B). Importantly, the rate of degradation of ZNF143 was increased upon ARF16-PB1 rescue when compared to cells not rescued with ARF16-PB1 (Figure 3C&D). To test whether ARF16-PB1 rescue affects the synthesis rate of ZNF143-AID, and thus contributing to the perceived degradation rate, we simultaneously blocked new protein synthesis with cycloheximide at the time of auxin treatment (Figure S5). Upon blocking protein synthesis, the ZNF143-AID protein degraded faster in the presence of ARF16-PB1 (Figure S5). Therefore, ARF expression promotes faster degradation kinetics and ARF does not influence protein synthesis rate.

Auxin Response Factor interacts with AID to rescue AID tag stability in mammalian cells.

To test the specificity of the ARF16-PB1 rescue, we mutated ARF16 residues within the interaction domain interface that are critical for its interaction with IAA17 (31, 32) (Figure 4A&B). We converted K944, D994, and D998 to Alanine in the ARF16-PB1-MT. In *Arabidopsis thaliana*, the corresponding mutations abolish ARF homodimerization and heterodimerization with IAA17 (32). We tested whether this mutant is capable of rescuing AID tagged protein stability in HEK293T-TIR1 cells. Chronic depletion of AID-tagged ZNF143 and TEAD4 was rescued with wild-type ARF16-PB1, but not with ARF16-PB1-MT (Figure 4C&D). However, we note that the ARF16-PB1 mutant protein is not as abundant as the wild type ARF16-PB1 (Figure 4C&D), presumably because dimerization can stabilize exogenous ARF16-PB1. This result suggests that rescue of stability is mediated by the interaction between ARF16-PB1 and AID. To confirm a physical interaction, we per-

formed a co-immunoprecipitation experiment. We found that NLS-mCherry-AID and eGFP-ARF16-PB1 interact in the absence of TIR1 (Figure 4E). However, the ARF16 mutations are sufficient to disrupt the ARF16/AID interaction (Figure 4E). The reciprocal IP confirmed the AID/ARF16-PB1 interaction and we were unable to detect an interaction of TIR1 with AID (Figure 4F). These data indicate that an ARF16-PB1/AID interaction mediates AID stability in the improved ARF-AID degron system.

Expression of ARF-PB1 and TIR1 prior to AID-tagging preserves native protein levels.

Rescuing chronic ZNF143 depletion does not result in full recovery of protein levels and approximately 25% of the genes that are differentially expressed in the chronic depletion remain dysregulated upon ARF-rescue (Figure 2D). To further improve the system and preserve native levels of the tagged protein, we constitutively expressed ARF16-PB1 prior to AID tagging. We generated a bicistronic construct with ARF-PB1 and TIR1 and an intervening P2A site, which separates the two proteins during translation. Genetic incorporation of this construct into the AAVS1 locus resulted in two independent clones that express ARF16-PB1 and TIR1 (Figure 5A). ZNF143 AID-tagging of both ARF-PB1/TIR1 HEK293T progenitor cell lines results in ZNF143 protein levels that are comparable to the parental lines (Figure 5B&C).

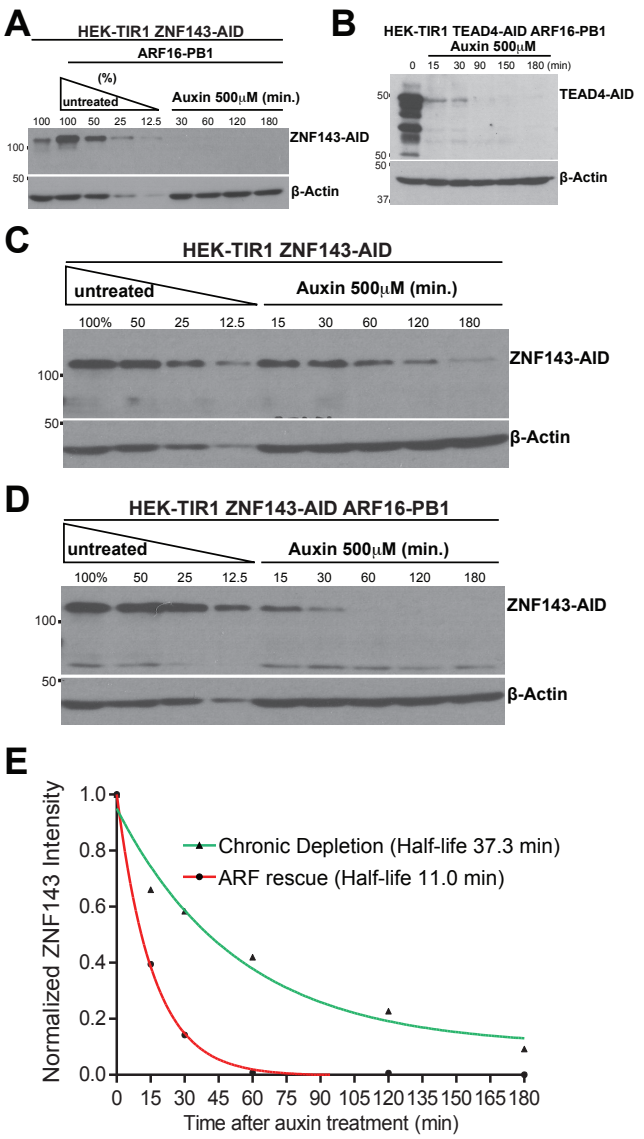

Fig. 3. ARF rescue promotes faster degradation kinetics upon addition of auxin. ZNF143 (A) and TEAD4 (B) are rapidly depleted upon auxin treatment. C) A quantitative Western blot measures the time dependent degradation of ZNF143-AID in the presence of 500μM auxin. Note that ZNF143 is chronically depleted in these cells and a longer exposure was needed to quantify auxin-induced reduction of ZNF143-AID levels. D) A quantitative Western blot measures 500μM auxin-induced ZNF143-AID degradation after ARF16-PB1 rescue. E) We measured the intensity of ZNF143-AID bands from panels C&D using densitometry and fit the data using nonlinear regression and a one-phase decay equation.

ZNF143 activates transcription in *cis*.

We directly and quantitatively assessed auxin-induced perturbation of ZNF143 by measuring genome-wide transcriptional changes upon auxin treatment. Conventional transcriptional profiling, such as RNA-seq, require mature RNA to accumulate or degrade to detect changes in transcription. Delayed detection poses a challenge when measuring the immediate transcriptional response upon rapid protein depletion. To overcome this limitation, we measured nascent RNA using PRO-seq (22–24). PRO-seq quantifies the immediate effect that degradation has upon transcribing RNA Polymerases. ZNF143 was first characterized as a sequence-specific activator as measured by reporter assays (36). In order to identify direct ZNF143 target genes and primary response genes, we performed genome-wide nascent RNA profiling after 90 minutes of auxin treatment in the chronically depleted and ARF-rescued ZNF143-AID cell lines. We define *primary effect genes* as immediately regulated upon rapid ZNF143 depletion and *direct gene targets* as primary response genes that ZNF143 regulates in *cis*. Many genes are activated and repressed upon auxin treatment in both backgrounds (Figure 6A). ZNF143 binding, as measured by ChIP-seq (37), is enriched proximal to the repressed gene class in the ARF rescue background (Kolmogorov–Smirnov two-sided p-value = $1.1e^{-16}$) and not the activated gene class (p-value = 0.047) (Figure 6B). In the chronic ZNF143 depletion background, the auxin-repressed gene class is not significantly closer to ZNF143 binding sites (p-value = 0.022) and genes within the activated gene class tend to be further away from ZNF143 binding sites (p-value = 0.0017) (Figure 6B). This supports recent genomic data, which found that many transcription factors (ER, GR, PPARγ, NFκB, HSF) specialize to exclusively activate or repress transcription in *cis* (38–45).

Transcription factors can direct bidirectional transcription at their binding sites (46, 47). Bidirectional transcription is a feature of gene promoters and enhancers (48) and a measure of regulatory element activity. We tested whether we could detect changes in bidirectional nascent RNA production upon ZNF143 depletion. We implemented a discriminative regulatory-element detection method (dREG) (49) to identify promoters and enhancers *de novo*. We performed differential bidirectional transcription analysis to identify

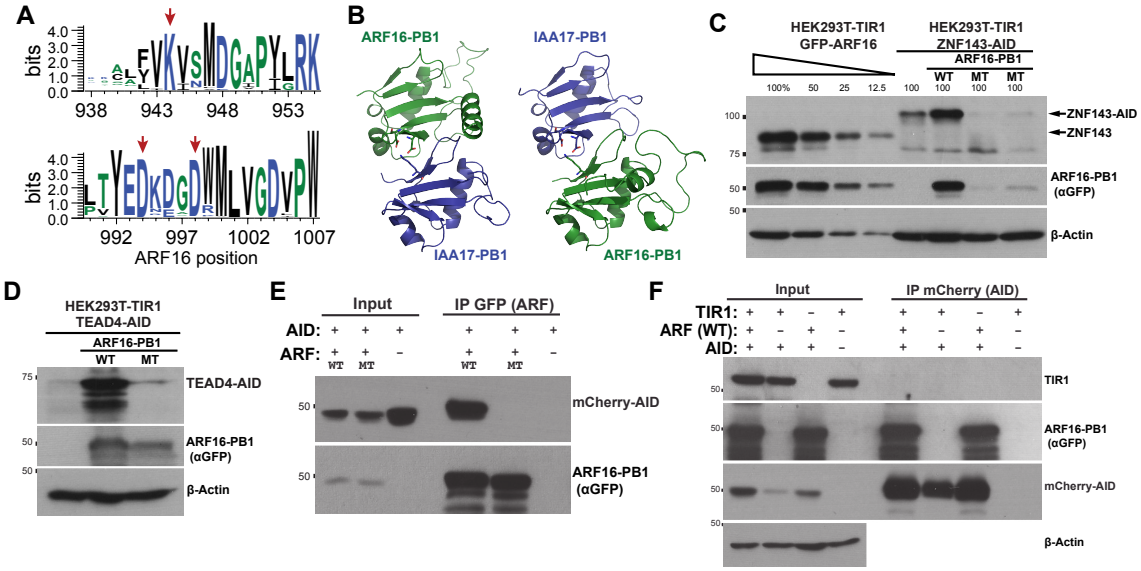

Fig. 4. The interaction of ARF-PB1 and AID mediates rescue of endogenous protein levels. A) Positions indicated by the red arrows are highly conserved within the AUX-IAA family (Pfam Family: PF02309). A seed alignment of the Aux-IAA family was generated using Pfam (33) and the resultant FASTA files were visualized using WebLogo (34). Positions on the x-axis are relative to ARF16 residue numbers. B) The amino acids D994 and D998 of ARF16 and K114 of IAA17 are shown in the left panel. The amino acid side chains corresponding to D183 and D187 of IAA17 and K944 if ARF16 are highlighted in the right panel. Note that IAA17/ARF16 heterodimeric complexes are shown in both orientations and that these domains of IAA17 and ARF16 are within the same protein domain family. IAA17 and ARF16 sequences were modeled (35) into each chain of an *Arabidopsis thaliana* ARF5 homodimeric structure (PDB entry: 4CHK (31)). These mutations in ARF16, which disrupt the electrostatic binding interface, fail to rescue chronic ZNF143 (C) and TEAD4 (D) degradation. E) These mutations disrupt this co-immunoprocipitation of mCherry-AID with eGFP-tagged ARF16-PB1. Consistent with lower stability of the ARF16-MT in panels C&D, the mutant GFP-ARF16-PB1 plasmid was transfected at a concentration three times higher than the wild type to achieve comparable expression of each protein. F) ARF16-PB1 is detected upon mCherry-AID immunoprecipitation, however we were unable to detect TIR1 associating with AID.

regulatory elements that increase and decrease transcriptional activity upon auxin treatment (Figure S6). Next, we performed *de novo* motif analysis (50) within the regulatory elements that increase or decrease bidirectional transcription. The canonical ZNF143 motif was exclusively found in the auxin-repressed regulatory elements (Figure 6C). Taken together with the integrative ChIP-seq/PRO-seq analysis from Figure 6A&B, we conclude that ZNF143 activates transcription of proximal genes and enhancers. These results serve as direct evidence that we are not only depleting ZNF143 protein levels, but we are functionally perturbing ZNF143 activity using the ARF-AID system.

ZNF143 targets are more responsive to perturbation upon ARF16 rescue.

Of the 168 genes that are classified as *repressed* upon auxin treatment in the ARF-rescue background, 167 genes have a net negative change in auxin-induced gene expression in the chronic depletion background (Figure S7A). Upon auxin treatment, eighty-seven percent (146/168) of the genes have a greater magnitude of response in the ARF-rescue background compared to chronic ZNF143-depleted cells (Figure S7A). These data show that the ARF-rescue is more sensitive to detect auxin-induced changes in ZNF143-dependent transcription compared to the chronically depleted background. Seventy-eight percent (57/73) of the auxin-repressed genes in the chronic ZNF143-depletion background are categorized as *repressed* in the rescue as well (Figure S7B); seventy percent (40/57) are repressed to a greater magnitude in the rescue (Figure S7B). This analysis indicates that expressing ZNF143 at near-endogenous levels is necessary to detect a robust transcriptional response

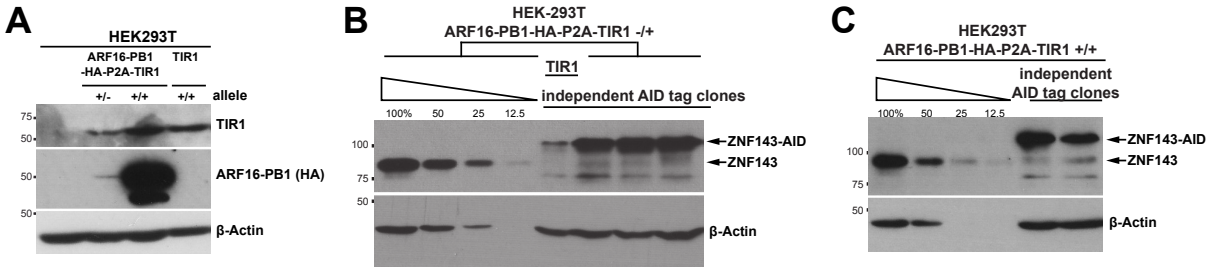

Fig. 5. Expression of ARF-PB1 prior to AID-tagging preserves ZNF143 protein levels. A) We generated two progenitor cell lines that express HA-tagged ARF16-PB1 and TIR1 from the same promoter, separated by a P2A site. Unmodified HEK293T cells are within lane 1. The construct is incorporated into at least one allele of AAVS1 (lane 2) and all AAVS1 alleles (lane 3). Note that HEK293T cells are not strictly diploid. Lane 4 is the original TIR1-expressing progenitor cell line. B) Three independent ZNF143-AID clones (lanes 6-8) have comparable protein levels as the heterozygous ARF-PB1/TIR1 progenitor cells. Consistent with previous figures, TIR1 expression alone compromises ZNF143-AID protein levels. C) Two independent ZNF143-AID clones (lanes 5&6) derived from the homozygous ARF-PB1/TIR1 cells preserve ZNF143 protein levels.

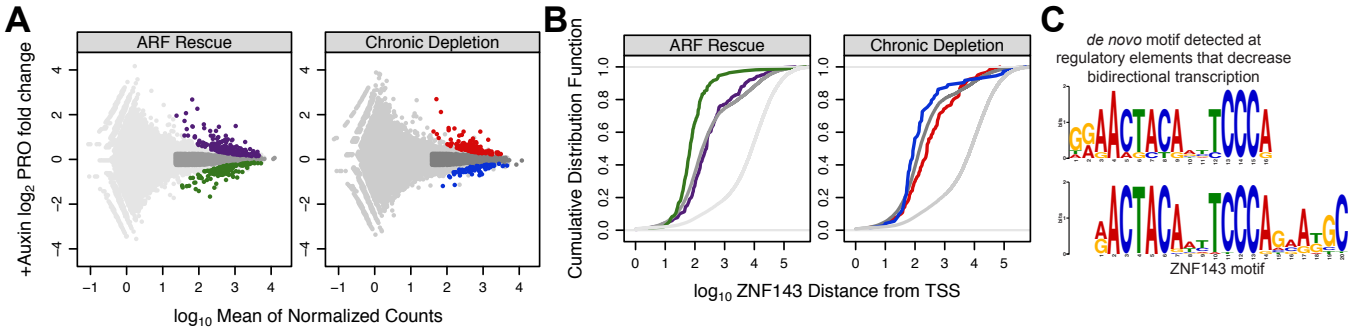

Fig. 6. ZNF143 is a canonical transcriptional activator. A) Genes are activated and repressed upon auxin treatment in both the chronic ZNF143-depleted background and the ARF-rescue of ZNF143 degradation background. Purple points are genes that increase expression and green genes decrease expression upon auxin treatment in the ARF-rescued background. Dark grey genes are expressed at comparable levels as activated and repressed genes, but they are confidently unchanged when auxin is added. B) Cumulative distribution plots quantify the relationship between the closest ZNF143 ChIP-seq peak and the start sites of genes within the regulated classes from panel A; trace colors correspond to panel A categories. ZNF143 binding sites are closer to auxin-repressed genes only in ARF-rescue background, suggesting that ZNF143 functions to activate transcription in *cis*. C) The ZNF143 motif was found *de novo* exclusively at regulatory elements that decrease bidirectional transcription upon auxin treatment.

upon ZNF143 depletion.

Auxin treatment activates the Aryl Hydrocarbon Receptor response.

In order to determine whether this system could be generally applied to study transcription factor function, we performed a control experiment to test whether auxin treatment alone affects transcription of human genes. Few genes are repressed upon auxin treatment (Figure S8A), regardless of FDR thresholds. However, over a range of FDR thresholds we consistently observe that the activated genes (Figure S8) are enriched in Aryl Hydrocarbon Receptor (AHR) binding sequences in their promoters and the most enriched pathway for this gene set is the Aryl Hydrocarbon Receptor pathway (q-value = 0.002) (51). We find that AHR binding (52) is enriched proximal to the activated gene class (p-value = $3.6e^{-11}$) and not the repressed gene class (p-value = 0.74) (Figure S8B&C). This control experiment highlights the importance of filtering aryl hydrocarbon receptor response genes from analyses when using any AID system to study transcriptional response.

ZNF143 regulates paused RNA Polymerase density.

Transcription can be regulated at various steps (53, 54), including chromatin opening (55–57), pre-initiation complex formation/stability and RNA Polymerase II (Pol II) recruit-

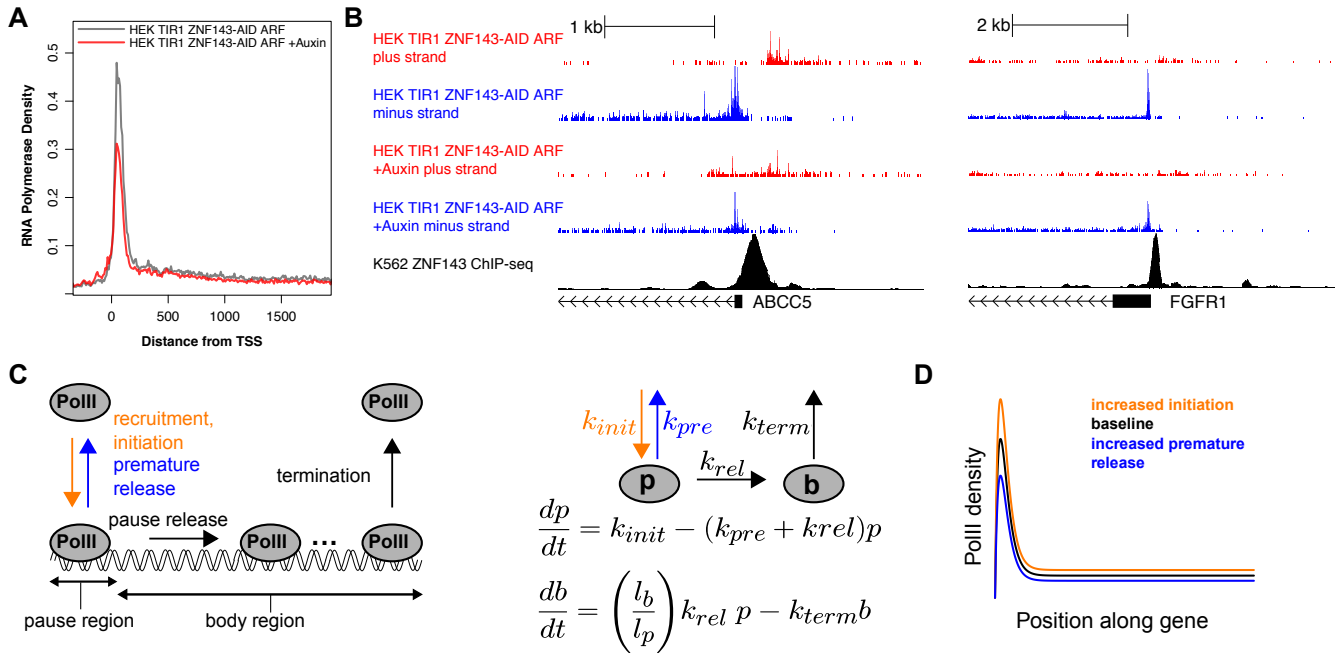

Fig. 7. ZNF143 regulates initiation/recruitment or pause stability. A) The composite profile of Pol II density at all auxin-repressed genes indicates that Pol II pause density is compromised upon ZNF143 depletion. B) Individual genes (ABCC5 and FGFR1) show compromised Pol II density in the pause region. C) Model structure and key variables are highlighted in this schematic. A mathematical formulation of the two component model in which *p* refers to Pol II density at the pause region and *b* refers to the density at the gene body region. D) This plot represents a steady state simulation for a reference model (black), a model in which transcriptional initiation was increased by 25% (orange), and a model in which premature pause release was increased by 60% (blue). The peak of the smooth curve was set to the steady state pause level and the plateau of the curve was set to the steady state gene body level. Note that this plot captures the preferential effect on the pause region as compared to the gene body region.

ment (58), Pol II initiation (59–61), Pol II pausing and release (62, 63), and elongation (64). General transcription machinery and cofactors directly catalyze these steps, but these factors are targeted to DNA by sequence-specific transcription factors, such as ZNF143. We sought to determine which transcription step(s) ZNF143 targets by characterizing the change in RNA Pol II profiles after rapid ZNF143 depletion (Figure S9). We found that the repressed gene class, which represents direct ZNF143 targets, show dramatic changes in the pause region compared to the gene body (Figures 7A&B, S10, and S11).

We implemented a mathematical modeling approach to better understand the potential mechanisms underlying decreased pause/body densities for repressed genes following ZNF143 inhibition. We formulated a two compartment model with dynamics for a pause region and gene body region. Model parameters include rate constants for transcriptional initiation/Pol II recruitment, premature pause release, pause release into productive transcription elongation, and termination of transcription (Figure 7C). We implemented parameter sensitivity analyses to determine if any model parameters could account for our experimental results. Our analysis showed that only changes in initiation and premature pause release could account for a large magnitude of Pol II density change in the pause region relative to the gene body. Increased initiation resulted in increases for both the pause region and the gene body region. In contrast, increases in premature release resulted in decreases for both the pause region and the gene body region (Figure 7D). These results suggest that decreases in the pause and gene body regions observed following ZNF143 inhibition could be accounted for by either decreases in initiation or increases in non-productive pause release. We used the model to further investigate the conditions under which the change in the pause region could be greater than the change in the gene body region for a variation in either the initiation or premature release rate. Our analysis showed that such preferential changes in the pause region will always be observed when the ratio of Pol II density in the pause region relative to the to the gene body, known as the pause index, is greater than a value of one. Moreover, the relative pause change was predicted by the model to be identical to the pause index, which is consistent with our result that the pause index at repressed genes is only modestly changed at genes that are repressed upon ZNF143 depletion (Figure S12). These combined experimental and modeling results suggest that ZNF143 regulates pausing density by facilitating RNA Polymerase II initiation or preventing premature dissociation of paused RNA Polymerase II.

Discussion

Expression of ARF-PB1 improves the auxin inducible degradation system. First, ARF-PB1 interacts with the AID-tagged protein to prevent degradation in the absence of auxin, thus the tagged protein's abundance is more representative of native levels. Secondly, the rate of auxin-induced depletion is increased in the ARF-AID system. We demonstrated the power of the ARF-AID system by rapidly depleting the transcription factor ZNF143 and quantifying genome-wide changes RNA Polymerase density.

Advantages of rapidly inducible degron systems.

Protein function can be studied by rapidly inducible degron systems in cases where translational fusion of the degron tag does not disrupt protein function or protein stability. These systems provide advantages in interpretation of protein function because measurements taken immediately after protein dysregulation can be attributed directly to the protein of interest. In contrast, other techniques that are general, such as RNAi and genetic knockout, do not provide opportunities to assay phenotypes immediately after protein depletion due to the gradual or chronic nature of dysregulation. The newly developed dTAG system (2) provides comparable advantages as ARF-AID and exogenous expression of two additional proteins is not required. Endogenous tagging of BRD4 with FKBP12^{F36V} dTAG did not result in dramatic protein depletion in the absence of the inducible degradation molecule, dTAG-13 (2). As the dTAG and ARF-AID systems become more widely adopted, we look forward to studies that systematically compare these different degron technologies.

We found that auxin treatment alone causes undesired transcriptional changes at AHR target genes, but it is unclear whether dTAG-13 treatment results in off-target changes in cellular phenotypes. These types of side effects can be abrogated by including proper control experiments and by depleting target proteins by multiple independent methods.

Possible mechanisms of ARF-mediated AID stabilization and rapid degradation.

ARF transcription factors are a critical component of the plant auxin-response system (65). Herein we find that ARF expression is an important component of engineered auxin-inducible degron systems. The ARF-AID system confers two distinct advantages 1) ARF expression limits auxin-independent degradation of target proteins and 2) ARF expression promotes more rapid auxin-inducible degradation of AID-tagged proteins. ARF and Aux/IAA proteins each harbor a conserved PB1 domain that can homodimerize or heterodimerize (6, 7). Mutations that interfere with ARF/AID interaction fail to rescue chronic, auxin-independent AID-degradation. TIR1 binds to domain II of Aux/IAA (10, 11) and ARF binds to domain III and IV; therefore, ARF and TIR1 do not directly compete for the same binding surface of Aux/IAA. Therefore, an ARF/AID interaction may cause conformational changes within AID that inhibit its interaction with auxin-unbound TIR1 (Figure 8).

Auxin-inducible degradation of ZNF143 is more rapid in the ARF-AID system. There are many plausible and non-mutually exclusive possibilities for the observed difference in degradation kinetics. The most simple explanation is that promoting the stability of the AID-tagged protein increases

its concentration, which directly affects degradation kinetics. Alternatively, ARF binding to AID may promote more efficient ubiquitination by exposing target residues to the auxin-bound TIR1 complex. ARF binding may cause allosteric changes in domain II of AID that promote a higher affinity interaction with auxin-bound TIR1 compared to ARF-unbound AID. Recent work has shown that different Aux/IAA proteins can interact with TIR1 in the absence of auxin to influence the association of auxin with TIR1 (66). Although we did not detect an interaction of TIR1 and IAA17 in Figure 4, we cannot dismiss such an interaction in cells. Therefore, the ARF-AID system may promote faster kinetics because ARF binding affects AID structure, which in turn modulates the affinity of TIR1 and auxin. Future studies and systematic comparisons are needed to determine the mechanisms that contribute to a more rapid auxin-inducible response.

Molecular functions of ZNF143.

Despite incredible advances in our understanding of the mechanisms of eukaryotic transcription and developments in systems biology, accurately predicting direct target genes and primary response genes of transcription factors remains a challenge. Proximal binding of a transcription factor to a gene is neither necessary nor sufficient to modulate gene expression. A fundamental question remains: how do transcription factors discriminate between genes in the genome in which to regulate? To begin to address this question we must first define the set of genes regulated by the transcription factor of interest. Technical limitations preclude experimentally identifying a comprehensive set of primary response genes for the vast majority of transcription factors, because we cannot rapidly induce or rapidly repress their activity. Perturbation methodologies that can be universally applied to any gene, such as RNAi, require days to efficiently deplete protein. This time-frame of depletion poses a major barrier to understanding transcription factor function, because secondary (and beyond) effects dominate conventional depletion/knockout methods. Herein, we show that applying the ARF-AID system to study transcription factor function overcomes these challenges.

The *Xenopus laevis* homolog of ZNF143, Staf (selenocysteine tRNA gene transcription activating factor), was first cloned and characterized nearly 25 years ago (36). This original report characterized the binding site of Staf within a regulatory element of the tRNA^{Sec} gene and char-

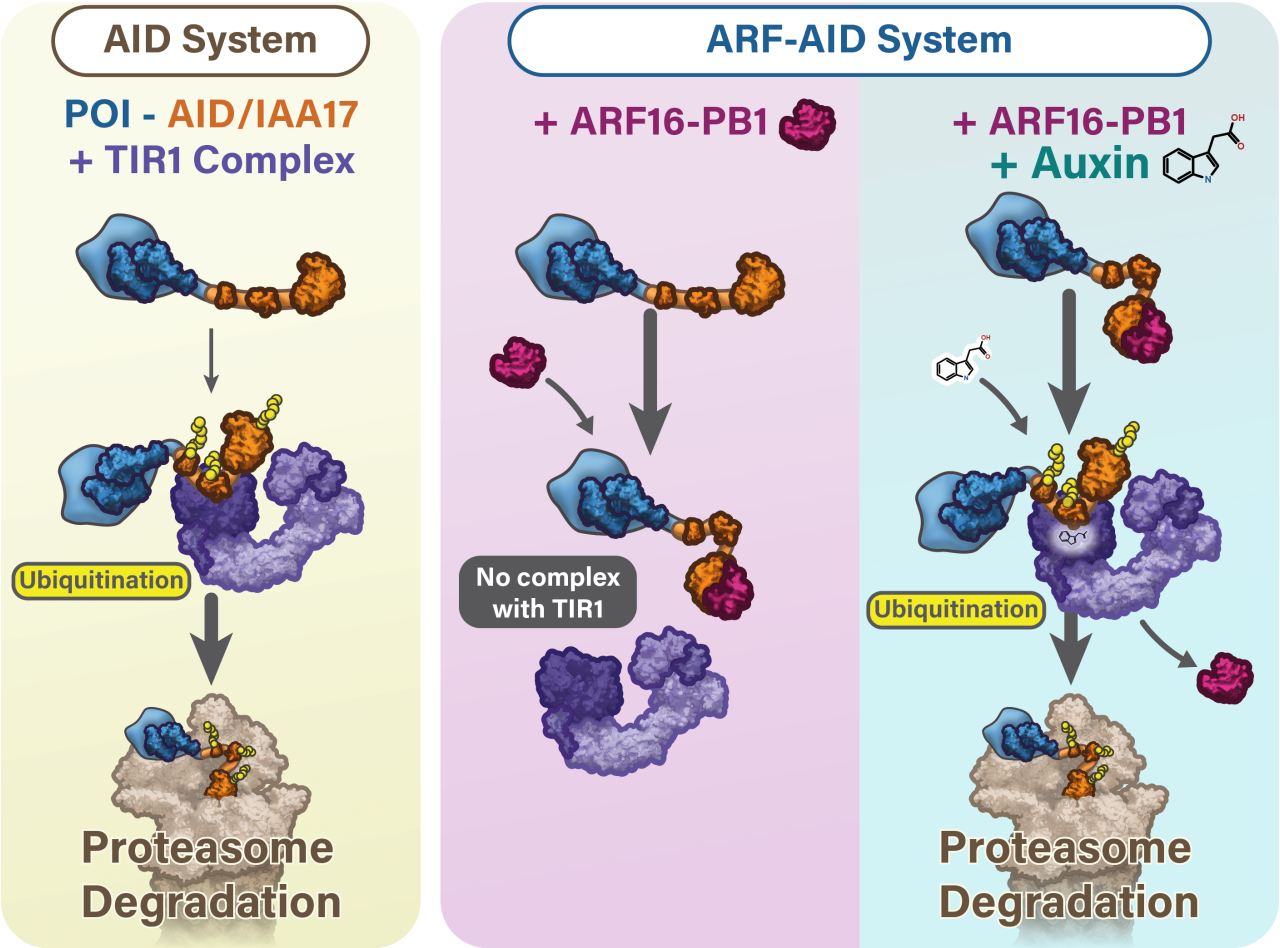

Fig. 8. The ARF-AID system preserves protein of interest (POI) expression levels in the absence of auxin and auxin treatment induces rapid degradation. A) The classical AID system can result in auxin-independent degradation of the AID tagged proteins. B) In the ARF-AID system, ARF-PB1 binds to AID to prevent TIR1 association with AID, which prevents auxin-independent AID degradation by the ubiquitin-mediated proteasomal pathway. Auxin facilitates the interaction of TIR1 with AID, promotes dissociation of ARF, and subsequent ubiquitination and proteasome-mediated degradation of the AID-tagged protein.

acterized the activator function of Staf using reporter assays (36). Recent transcriptional profiling upon siRNA-mediated ZNF143 depletion identified many activated and repressed genes (67). ZNF143 depletion caused twice as many genes to decrease expression relative to the number of genes that increased expression. The authors concluded that ZNF143 is primarily an activator, but they note that ZNF143 may be involved in repression. Our results corroborate the activation function of ZNF143 and indicate that although many genes are activated upon immediate ZNF143 depletion, ZNF143 does likely not act in *cis* to mediate repression. Importantly, we inhibited ZNF143 for only 90 minutes and we measured nascent RNA levels, so the repressive role of ZNF143 cannot be attributed to the post-primary response of ZNF143 dysregulation. Alternative mechanisms of immediate indirect repression, such as squelching (40, 43, 44), may be responsible for the observed repressive role of ZNF143. We further characterized ZNF143's role in activation and found that ZNF143 functions to control paused RNA Pol II density. Mathematical modeling indicates that ZNF143 either positively regulates RNA Polymerase initiation or prevents non-productive dissociation of paused Pol II.

ZNF143 is also involved in chromatin looping of distal enhancers to promoters (68). Enhancer-promoter looping frequently and preferentially occurs at promoters containing paused RNA Pol II (69). Therefore, we propose a model whereby ZNF143 directly regulates the amount of paused Pol II on a given promoter, which facilitates enhancer looping.

Rapidly inducible systems, such as hormone signaling and heat shock response, have contributed greatly to our understanding of transcriptional regulation. The success of these models, in part, is because the regulatory processes can be triggered instantaneously and tracked. New technologies and inhibitors that permit rapid and specific protein dysregulation promise to revolutionize the study of complex regulatory mechanisms.

Methods

Cell lines.

HEK293T cells were purchased from ATCC and were grown in DMEM with 10% FBS, Penicillin/Streptomycin and 5% glutamine. MCF7 cells were purchased from ATCC and were grown in DMEM with 10% FBS and Penicillin/Streptomycin. CENP-I-AID-eGFP DLD1-OsTIR1 cells were generated in Ian Cheeseman's lab (70) and grown in RPMI1640 media with 10% FBS and Penicillin/Streptomycin.

Plasmids and constructs.

OsTIR1 was integrated into AAVS1 locus of the HEK293T cells using the CMV-OsTIR1-PURO plasmid from Masato Kanemaki (pMK232, Addgene #72834) (21). OsTIR1 was integrated into the genome by CRISPR-Cas9 mediated repair using an sgRNA targeting AAVS1 safe harbor locus cloned into pSpCas9(BB)-2A-GFP from Feng Zhang (PX458, Addgene #48138) (20, 21, 71). The ARF16-PB1 domain (amino acid 878-1055) and ARF25 (MR and PB1 domain, amino acid 369-889, Os12t0613700-01) genes were codon optimized for humans and synthesized from Bio Basic Inc, New York. A nuclear localization signal (NLS) was added at the N-terminus of the ARF16-PB1 domain. These genes were inserted into eGFP-C2 vector digested with XhoI and HindIII by cold fusion cloning (System Biosciences). The CMV-OsTIR1-PURO plasmid was digested with AfeI and we inserted the codon optimized ARF16-PB1 domain separated by P2A from OsTIR1 to generate the ARF16-PB1-HA-P2A-OsTIR1 construct. This plasmid was co-transfected with AAVS1 sgRNA and we selected puromycin resistant clones to generate the homozygously integrated transgenic cell line. The resulting transgenic HEK293T-TIR1 and ARF16-PB1-HA-P2A-OsTIR1 cell lines were used to tag transcription factors with AID tag using the CRISPR-Cas9 system. The NLS-mCherry-AID plasmid was constructed by digesting pCDNA5 vector with PmeI enzyme and inserted the NLS-mCherry-AID fragment using cold fusion cloning (System Biosciences).

Endogenous AID tagging in HEK293T cells.

Endogenously AID tagged TEAD4, ZNF143 and p53 cells were generated using CRISPR mediated gene editing. sgRNAs that target the 3′ end of the respective coding sequences were cloned into hSpCas9 plasmid (PX458, Addgene Plasmid #48138) (71). The linear donor was generated by PCR and gel purified from a plasmid harboring a synthetic AID-P2A-Hygromycin insert (Bio Basic Inc.). We amplified the insertion using primers that contain 50 nucleotide homology tails. The primers contained 5′ phosphorothioate modifications to increase PCR product stability in the cell (72). The primers used for making PCR donor fragments are reported in Table 1. HEK293T cells were co-transfected with 1 μg of CRISPR/Cas9-sgRNA plasmid and 400 ng of linear donor PCR product using Lipofectamine 3000 in a 6 well plate. Cells were expanded into 10 cm plates two days after transfection. The knock-in cells were selected by treating with 200 μg/ml Hygromycin B three days after transfection. Individual clones were selected and confirmed by Western blotting and Sanger sequencing of PCR amplicons. The sgRNAs from Table 2 were used for targeting the 3′ end (C-terminus of the protein) of the indicated genes.

EGFP-ARF16-PB1 stable cell lines.

We transfected plasmids expressing NLS-ARF16-PB1 fused with eGFP at the C-terminus or eGFP-NLS-ARF16-PB1K944A, D994A, D998A mutant into each of the following: HEK293T, HEK293T-TIR1, and HEK293T-TIR1 cells where either TEAD4 or ZNF143 were AID-tagged. Cells were expanded for one week and GFP-sorted iteratively (three times) until we obtained a stable population of GFP expressing cells.

Immunoprecipitation and immunoblotting.

HEK293T or HEK293T-TIR1 cells were co-transfected with mCherry-NLS-AID and eGFP-ARF16-PB1 or eGFP-ARF16-PB1 mutant plasmids. The mutant eGFP-ARF16-PB1 plasmid was co-transfected at a concentration three times higher than the wild type to get comparable expression of the mutant protein. The co-IP data from Figure 4 was generated by separately transfecting mCherry-AID into HEK293T, HEK293T-eGFP-ARF16-PB1, and HEK293T-TIR1-eGFP-ARF16-PB1 cells. Cells were lysed 24 hours post-transfection in a buffer containing 50 mM Tris (pH 7.5), 150 mM NaCl, 0.5% NP-40, 1 mM EDTA, and protease and phosphatase inhibitors for 30 minutes on ice and then sonicated 30 seconds on and 30 seconds off for 15 cycles. Lysate was clarified by centrifugation for 15 minutes at 12000g in 4°C. Anti-GFP antibody conjugated magnetic beads (Chromotek, gtma-10) or anti-mCherry conjugated affinity gel (Biolegend, 689502) were blocked with 1% BSA for 15 minutes. The beads were incubated with clarified lysate for 1.5 hours at 4°C. The immunoprecipitate was recovered with DynaMag racks or by centrifuging at 3000xg for 1 minute. Beads were washed for 5 minutes three times in the lysis buffer and 60 μl 2X Laemmli buffer was added directly to the beads. The complex was heat denatured at 95°C for 5 minutes. We used the following antibodies for the western blots: anti-GFP (gift from Daniel Foltz, Northwestern University), anti-mCherry (1:5000, Rabbit, abcam, ab183628), ZNF143 (1:5000, H00007702-MO1, Abnova), TEAD4 (1:1000, sc-101184, Santa Cruz), p53 (1:1000, DO1, Santa Cruz), anti-TIR1 1: 10,000, gift from Masato Kanemaki, Osaka University), β-Actin (1:5000, Sigma A1978), β-Tubulin (AA2, gift from Todd Stukenberg, University of Virginia), CENP-I (Rabbit, gift from Todd Stukenberg, University of Virginia). Regression lines for kinetic data were fit using GraphPad Prism (73).

Drug treatment.

Cells were treated with 10 μM MG132 for 4.5 hours to test whether AID-tagged proteins were degraded through the proteasome pathway. A stock of 50 mM Auxin was diluted to a final concentration of 500 μM auxin in the culture media. The 50 mM stock was solubilized in DMSO for the 3 hour auxin treatment PRO-seq experiments using the progenitor line. For all other experiments, the 50 mM auxin was solubilized in water. A Degradation rate upon auxin treatment was measured by treating cells with 10 μg/ml cycloheximide and 500 μM Auxin and collecting samples at every 15 minutes for 4 hours.

PRO-seq library preparation.

Cell permeabilization was performed as previously described (23). Cells were collected in 10 ml ice cold PBS after trypsinization and then collected and washed in 5 ml buffer W (10 mM Tris-HCl pH 7.5, KCl 10 mM, Sucrose 150 mM, 5 mM $MgCl_2$, 0.5 mM $CaCl_2$, 0.5 mM DTT, 0.004 units/ml SUPERaseIN RNase inhibitor (Invitrogen), Protease inhibitors (cOmplete, Roche)). The washed cells were then permeabilized with buffer P (10 mM Tris-HCl pH 7.5, KCl 10 mM, Sucrose 250 mM, 5 mM $MgCl_2$, 1 mM EGTA, 0.05% Tween-20, 0.1% NP40, 0.5 mM DTT, 0.004 units/ml SUPERaseIN RNase inhibitor (Invitrogen), Protease inhibitors (cOmplete, Roche)) for 3 minutes. Cells were washed again with 10 ml buffer W before transferring into 1.5 ml tubes using wide bore pipette tips. Finally, cells were re-suspended in 500 μl buffer F (50 mM Tris-HCl pH 8, 5 mM $MgCl_2$, 0.1 mM EDTA, 50% Glycerol and 0.5mM DTT). After counting the nuclei, we generated 50 μl aliquots with approximately 3-5 x 10^5 cells that were snap frozen in liquid nitrogen and stored at -80°C. All centrifugations were done at 500xg for 10 ml conical tubes and 2000xg for 1.5 ml tubes at 4°C and all buffers were maintained on ice. PRO-seq libraries were prepared as described previously (39), with the following modifications. The libraries were amplified by PCR for a total of 10 cycles. We performed 5′ de-capping using RppH, 5′ hydroxyl repair, 5′ adapter ligation, and reverse transcription while the 3′ RNA biotin moiety was bound to magnetic streptavidin beads. We added an eight base random unique molecular identifier to the 5′ end of the adapter that is ligated to the 3′ end of the nascent RNA. We did not perform any size selection because we were willing to tolerate excessive adapter/adapter ligation products to ensure that our libraries were not biased against short nascent RNA insertions.

PRO-seq analyses.

We removed adapters from the paired end 1 or single end reads using `cutadapt` (74). Each 3′ adapter harbored an 8 base unique molecular identifier (UMI). We removed PCR duplicates based on the UMIs using `fqdedup` (75). We trimmed UMIs with `fastx_trimmer` (76) and we im-

Name	Sequence
ZNF143F	A*A*GAAGCCATCAGAATAGCGTCTAGAATCCAACAAGGAGAAACGCCAGGGCTTGACGACGGTGGATCTGGAGGTTCAGGTGGCAGTGTCGAGCTGAATCT
ZNF143R	A*A*GACTCCTTCTGCTTTATTGCTCCATTGTTCTGAGGATTAATCATCCAATCAGTTAGCCTCCCCCATCTC
TEAD4F	T*G*TCTTTGAGGTGTCAGCCAGTGAGCACGGGGCTCAGCACCACATCTACAGATTAGTTAAGGAGGGTGGATCTGGAGGTGGCAGTGTCGAGCTGAATCT
TEAD4R	C*G*TCTCTTCCCCCCTCCCTGCTCCCCGAGTCTCTCATTCTTTCACCAGCCTCAGTTAGCCTCCCCCATCTC
p53F	A*G*TCTACCTCCCGCCATAAAAAACTCATGTTCAAGACAGAAGGGCCTGACTCTGATGGTGGATCTGGAGGTTCAGGTGGCAGTGTCGAGCTGAATCT
p53R	G*G*GGTGGGAGGCTGTCAGTGGGGAACAAGAAGTGGAGAATGTCAGTCTGATCAGTTAGCCTCCCCCATCTC

Table 1. PCR Homology Donor Construct Primers

Name	Sequence
TEAD4	TCAGCACCACATCTACAGGC
ZNF143	GAGGATTAATCATCCAACCC
p53	GGAGAATGTCAGTCTGAGTC

Table 2. sgRNA Primers (DNA target sequence)

plemented `fastx_reverse_complement` to generate the reverse complement sequence (76). We aligned reads to *hg38* with `bowtie2` (77). We sorted aligned *BAM* files using `samtools` (78). We used `seqOutBias` to generate *bigWig* files (79). We used the `bigWig` R package (80) and UCSC Genome Browser Utilities (81) to query *bigWig* files within genomic coordinates. `Bedtools` was used to parse genomic coordinate files and query for overlapping regions (82). Differential nascent transcript abundance was measured by `DESeq2` (83). Bidirectional transcription was identified using `dREG` (49). `MEME` was used for *de novo* motif discovery within dREG-identified regulatory elements that change upon ZNF143 depletion; `TOMTOM` matched the ZNF143 motif (84) to a database that is curated by `HOMER` (85). All the analysis details and code are available at https://github.com/mjg54/znf143_pro_seq_analysis. Raw sequencing files and processed *bigWig* files are available from GEO accession record GSE126919.

Model formulation.
The dynamics for the concentrations or densities of RNA Polymerases at pausing regions and gene bodies, defined as p and b, are described as follows:

$$\frac{dp}{dt} = k_{init} - (k_{pre} + k_{rel})\, p$$

$$\frac{db}{dt} = \left(\frac{l_p}{l_b}\right) k_{rel}\, p - k_{term}\, b$$

where k_{init} is the rate of transcription initiation, k_{pre} is the rate constant for premature paused Pol II release, k_{rel} is the rate constant for the release of a paused Pol II as transcription proceeds into productive elongation in the gene body, and k_{term} is the rate constant for transcription termination. The term l_p/l_b is a ratio of the relative DNA segment lengths that is applied to adjust the gene body concentration based on the larger amount of DNA in the gene body as compared to the pause region. The term k_{init} implicitly accounts for the product of the unbound Pol II concentration and the rate constant for initiation. Concentration is considered as number of RNA polymerases per length of DNA. Thus this concentration is referred to as a density. We consider this model as though the units are dimensionless for the analysis of how specific rates influence the relative Pol II quantities at pause sites and within the gene bodies. The steady state levels (p_{ss}, b_{ss}) are found by setting $dp/dt = db/dt = 0$. Because understanding the effects of the relative pause region length is not our focus, we set $r = l_p/l_b$ for the parameter sensitivity analyses.

$$p_{ss} = \frac{k_{init}}{k_{pre} + k_{rel}}$$

$$b_{ss} = \frac{r\, k_{rel}}{k_{term}}\, p_{ss} = \frac{r\, k_{rel}\, k_{init}}{k_{term}\, (k_{pre} + k_{rel})}$$

The pause index is the relative density of reads in the pause region compared to the gene body ($P_i = p_{ss}/b_{ss}$). The pause index is only dependent on k_{term} and k_{rel}, the rate constants for the termination of transcription and release into productive gene body elongation:

$$P_i = \frac{k_{term}}{r\, k_{rel}}$$

Parameter sensitivity analysis.
To examine the effects of each parameter on the pause and body concentrations, we considered high and low parameter values ($k^{(hi)}$ and $k^{(lo)}$) and computed the changes in p_{ss} and b_{ss}. The following notation documents the change in p_{ss} when k is changed from a relatively high to a relatively low value: $\Delta p(k) = p_{ss}(k^{(hi)}) - p_{ss}(k^{(lo)})$). First, we evaluate the effects of the transcription initiation rate (k_{init}) on the steady state pause region and gene body Pol II concentrations.

$$\Delta p(k_{init}) = \frac{k_{init}^{(hi)} - k_{init}^{(lo)}}{k_{pre} + k_{rel}}$$

$$\Delta b(k_{init}) = \frac{r\, k_{rel} \left(k_{init}^{(hi)} - k_{init}^{(lo)}\right)}{k_{term}\, (k_{pre} + k_{rel})}$$

Note that $k^{(hi)} > k^{(lo)}$ by definition, so that $\Delta p(k_{init}) > 0$ and $\Delta b(k_{init}) > 0$. Therefore, increasing the rate of transcription initiation will result in both pause region and gene body increases. We present results of single parameter changes that can also be considered using a standard sensitivity analysis. For this example the sensitivities are computed as follows:

$$\frac{\partial p_{ss}}{\partial k_{init}} = \frac{1}{k_{pre} + k_{rel}} > 0$$

$$\frac{\partial b_{ss}}{\partial k_{init}} = \frac{r\, k_{rel}}{k_{term}\, (k_{pre} + k_{rel})} > 0$$

In general, $\Delta p(k) \sim (\partial p/\partial k)(k^{(hi)} - k^{(lo)})$ for small changes in k and $sign(\Delta p(k)) = sign(\partial p/\partial k)$. Next we consider the effects of varying the rate constant for premature pause release (k_{pre}).

$$\Delta p(k_{pre}) = \frac{k_{init}\left(k_{pre}^{(lo)} - k_{pre}^{(hi)}\right)}{\left(k_{pre}^{(hi)} + k_{rel}\right)\left(k_{pre}^{(lo)} + k_{rel}\right)}$$

$$\Delta b(k_{pre}) = \frac{r\, k_{rel}\, k_{init}\left(k_{pre}^{(lo)} - k_{pre}^{(hi)}\right)}{k_{term}\left(k_{pre}^{(hi)} + k_{rel}\right)\left(k_{pre}^{(lo)} + k_{rel}\right)}$$

These results show that increasing the rate constant for premature pause release will decrease both pause region and gene body Pol II concentrations ($\Delta p(k_{pre}) < 0$ and $\Delta b(k_{pre}) < 0$). We next demonstrate that an increase in the rate constant for the release of Pol II into the gene body (k_{rel}) decreases p_{ss} and increases b_{ss}:

Parameter increased	Change in p_{ss}	Change in b_{ss}
k_{init}	increase	increase
k_{pre}	decrease	decrease
k_{rel}	decrease	increase
k_{term}	no change	decrease

Table 3. Parameter sensitivity summary

$$\Delta p(k_{rel}) = \frac{k_{init}\left(k_{rel}^{(lo)} - k_{rel}^{(hi)}\right)}{\left(k_{pre} + k_{rel}^{(hi)}\right)\left(k_{pre} + k_{rel}^{(lo)}\right)}$$

$$\Delta b(k_{rel}) = \frac{r\ k_{init}\ k_{pre}\left(k_{rel}^{(hi)} - k_{rel}^{(lo)}\right)}{k_{term}\left(k_{pre} + k_{rel}^{(hi)}\right)\left(k_{pre} + k_{rel}^{(lo)}\right)}$$

It is interesting to note that if there is no premature pause release (i.e., $k_{pre} = 0$), the model predicts that a change in the rate of pause release into transcriptional elongation will not affect the concentration of RNA polymerases in the gene body, if all other factors are identical (i.e., $\Delta b(k_{rel}) = 0$ for $k_{pre} = 0$). Finally, we evaluate the effect of modifying the rate constant for the termination of transcription:

$$\Delta p(k_{term}) = 0$$

$$\Delta b(k_{term}) = \frac{r\ k_{init}\ k_{pre}\left(k_{term}^{(lo)} - k_{term}^{(hi)}\right)}{k_{term}^{(hi)} k_{term}^{(lo)}\left(k_{pre} + k_{rel}\right)}$$

These results shows that an increase in the rate constant for transcriptional termination does not affect the steady state level of paused Pol II but will decrease the gene body concentration of RNA polymerases ($\Delta p(k_{term}) = 0$, $\Delta b(k_{term}) < 0$). The results from our parameter sensitivity analyses are illustrated in Table 3 where the entries for p_{ss} and b_{ss} indicate the effect of increasing each parameter.

Relative effects of transcriptional initiation and premature release on Pol II distribution.

Our preceding analyses show that consistent changes in the pause region and gene body (i.e., both either increase or decrease) are only observed following changes in the rate of transcriptional initiation or the rate constant for premature pause release (k_{init}, k_{rel}). Our experimental data show that repressed genes show decreases in both the pause region and the gene body region. These decreases in Pol II density were greater in the pause region in comparison to the gene body. Next, we document the conditions under which the effects of varying the rates of initiation and premature release of the paused Pol II are greater for the pause region as compared to the gene body (e.g., $\Delta p(k_{init}) > \Delta b(k_{init})$). Changes in transcriptional initiation are set as $k_{init}^{(hi)} - k_{init}^{(lo)} = \Delta k$:

$$\frac{\Delta k}{k_{pre} + k_{rel}} > \frac{r\ k_{rel}\ \Delta k}{k_{term}\ (k_{pre} + k_{rel})}$$

This condition is satisfied for $\frac{l_b}{l_p} > \frac{k_{rel}}{k_{term}}$ (recall $r = l_p/l_b$). In general, l_b/l_p is a large value because the pause region (<100 bp) is much smaller than the gene body (approximately >10 kb). So $k_{rel}/k_{term} < l_b/l_p \sim 100$ must be obtained. For changes in premature release, the condition is as follows:

$$\frac{k_{init}(-\Delta k)}{\left(k_{pre}^{(hi)} + k_{rel}\right)\left(k_{pre}^{(lo)} + k_{rel}\right)} > \frac{r\ k_{rel}\ k_{init}(-\Delta k)}{k_{term}\left(k_{pre}^{(hi)} + k_{rel}\right)\left(k_{pre}^{(lo)} + k_{rel}\right)}$$

This relation leads to the same constraint observed for k_{init}: $k_{rel}/k_{term} < l_b/l_p$. Recall that the pause index is defined as $P_i = k_{term}/r\ k_{rel} = (l_b/l_p)(k_{term}/k_{rel})$. Therefore, $P_i > 1$ for the same condition that constrains $\Delta p(k_{pre}) > \Delta b(k_{pre})$ for changes in k_{init} and k_{pre}: $k_{rel}/k_{term} < l_b/l_p$. This demonstrates that, for an arbitrary change in either the initiation rate or the premature pause release rate constant, the effect of the change in the pause region will be greater than the change in the gene body region whenever the pause region Pol II concentration is greater than that at the gene body. Further, the effect ratio is identical for changes in k_{init} and k_{rel} and is equal to the value of the pause index: $\Delta p/\Delta b = P_i$.

Pause region and gene body model visualization.

We aimed to generate plots in which steady state levels of pause region and gene body concentration were imposed upon the peak and flat regions of a profile that is characterized by an exponential approach towards the peak followed by an exponential decay towards a stable plateau. We used a sum of exponential functions for the waveform:

$$density(bp) = \frac{pk_{pause}}{pk}\left(\frac{bp}{\tau} exp\left(\frac{-(bp-\tau)}{\tau}\right) + pk_{body}\left(1 - exp\left(\frac{-bp}{\tau}\right)\right)\right)$$

where bp (base pairs) is the independent variable and τ is the exponential decay constant. The parameter pk is set to the root of the derivative as shown below so that pk_{pause} determines the peak of the waveform. The parameter pk_{body} is set such that the asymptotic gene body region decays to a desired level. The derivative of this waveform is

$$\frac{d}{dt} density(bp) = \frac{pk_{pause}}{pk}\left(\frac{pk_{body}}{\tau} e^{-bp/\tau} - \frac{bp}{\tau^2} e^{(\tau - bp)/\tau} + \frac{1}{\tau} e^{(\tau - bp)/\tau}\right)$$

and the root of the derivative is given by the value of bp at the peak of the waveform ($max(density)$):

$$bp = \frac{\tau(pk_{body} + e)}{e}$$

For $bp >> \tau$, the gene body level assymptotically approaches $pk_{body}\ pk_{pause}/pk$. We implicitly determine a value for pk_{body} that will give a gene body level of a desired level. We select a value of pk_{body} that will give a plateau $pk_{body}\ pk_{pause}/pk$ of choice for a given setting of the pause peak pk_{pause}. After implicitly finding a value for pk_{body}

that produces the gene body level of choice, the waveform is produced.

ACKNOWLEDGEMENTS
This work was funded by R35-GM128635 to MJG. We thank Dr. Ricardo Henriques for making the bioRχiv LaTeX template publicly available. We thank Arun Dutta and Drs. Anindya Dutta, Todd Stukenberg and Prasad Trivedi for discussion and comments. Dr. Ryan Lewis from http://scidelight.com/ illustrated Figures 1A, 8, S1, and S3D.

AUTHOR CONTRIBUTIONS
KMS conceived of the ARF-AID hypothesis. KMS and BDM performed the experiments. WA implemented the mathematical models. FMD, LJC, and MJG developed the PRO-seq protocol. KMS and MJG conceptualized and developed the project. KMS and MJG designed the experiments. MJG and KMS analyzed the data. MJG supervised the project. MJG acquired the resources and funding. KMS, WA, and MJG wrote the original draft. KMS, BDM, WA, FMD, LJC, and MJG edited the manuscript.

Bibliography

1. Kohei Nishimura, Tatsuo Fukagawa, Haruhiko Takisawa, Tatsuo Kakimoto, and Masato Kanemaki. An auxin-based degron system for the rapid depletion of proteins in nonplant cells. *Nature methods*, 6(12):917, 2009.
2. Behnam Nabet, Justin M Roberts, Dennis L Buckley, Joshiawa Paulk, Shiva Dastjerdi, Annan Yang, Alan L Leggett, Michael A Erb, Matthew A Lawlor, Amanda Souza, et al. The dtag system for immediate and target-specific protein degradation. *Nature chemical biology*, 14(5):431, 2018.
3. Meirav Lavy and Mark Estelle. Mechanisms of auxin signaling. *Development*, 143(18): 3226–3229, 2016.
4. Luz Irina Calderon-Villalobos, Xu Tan, Ning Zheng, and Mark Estelle. Auxin perception—structural insights. *Cold Spring Harbor perspectives in biology*, page a005546, 2010.
5. Si-Bei Li, Zong-Zhou Xie, Chun-Gen Hu, and Jin-Zhi Zhang. A review of auxin response factors (arfs) in plants. *Frontiers in plant science*, 7:47, 2016.
6. Jungmook Kim, Klaus Harter, and Athanasios Theologis. Protein–protein interactions among the aux/iaa proteins. *Proceedings of the National Academy of Sciences*, 94(22): 11786–11791, 1997.
7. Tim Ulmasov, Gretchen Hagen, and Tom J Guilfoyle. Dimerization and dna binding of auxin response factors. *The Plant Journal*, 19(3):309–319, 1999.
8. Heidi Szemenyei, Mike Hannon, and Jeff A Long. Topless mediates auxin-dependent transcriptional repression during arabidopsis embryogenesis. *Science*, 319(5868):1384–1386, 2008.
9. Shiv B Tiwari, Gretchen Hagen, and Tom J Guilfoyle. Aux/iaa proteins contain a potent transcriptional repression domain. *The Plant Cell*, 16(2):533–543, 2004.
10. William M Gray, Stefan Kepinski, Dean Rouse, Ottoline Leyser, and Mark Estelle. Auxin regulates scf tir1-dependent degradation of aux/iaa proteins. *Nature*, 414(6861):271, 2001.
11. Nihal Dharmasiri, Sunethra Dharmasiri, Alan M Jones, and Mark Estelle. Auxin action in a cell-free system. *Current Biology*, 13(16):1418–1422, 2003.
12. Magdalena Morawska and Helle D Ulrich. An expanded tool kit for the auxin-inducible degron system in budding yeast. *Yeast*, 30(9):341–351, 2013.
13. Kohei Nishimura and Tatsuo Fukagawa. An efficient method to generate conditional knockout cell lines for essential genes by combination of auxin-inducible degron tag and crispr/cas9. *Chromosome Research*, 25(3-4):253–260, 2017.
14. Ewelina Zasadzińska, Jiehuan Huang, Aaron O Bailey, Lucie Y Guo, Nancy S Lee, Shashank Srivastava, Kelvin A Wong, Bradley T French, Ben E Black, and Daniel R Foltz. Inheritance of cenp-a nucleosomes during dna replication requires hjurp. *Developmental cell*, 47(3):348–362, 2018.
15. Kara L McKinley, Nikolina Sekulic, Lucie Y Guo, Tonia Tsinman, Ben E Black, and Iain M Cheeseman. The cenp-ln complex forms a critical node in an integrated meshwork of interactions at the centromere-kinetochore interface. *Molecular cell*, 60(6):886–898, 2015.
16. Sebastian Hoffmann, Marie Dumont, Viviana Barra, Peter Ly, Yael Nechemia-Arbely, Moira A McMahon, Solène Hervé, Don W Cleveland, and Daniele Fachinetti. Cenp-a is dispensable for mitotic centromere function after initial centromere/kinetochore assembly. *Cell reports*, 17(9):2394–2404, 2016.
17. Shengya Cao, Keda Zhou, Zhening Zhang, Karolin Luger, and Aaron F Straight. Constitutive centromere-associated network contacts confer differential stability on cenp-a nucleosomes in vitro and in the cell. *Molecular biology of the cell*, 29(6):751–762, 2018.
18. Gonzalo I Mendoza-Ochoa, J David Barrass, Barbara R Terlouw, Isabella E Maudlin, Susana de Lucas, Emanuela Sani, Vahid Aslanzadeh, Jane AE Reid, and Jean D Beggs. A fast and tuneable auxin-inducible degron for depletion of target proteins in budding yeast. *Yeast*, 2018.
19. Kumiko Samejima, Hiromi Ogawa, Alexander V Ageichik, Kevin L Peterson, Scott H Kaufmann, Masato T Kanemaki, and William C Earnshaw. A cell suicide module: Auxin-induced rapid degradation of inhibitor of caspase activated dnase (icad) induces apoptotic dna fragmentation, caspase activation and cell death. *Journal of Biological Chemistry*, pages jbc–M114, 2014.
20. Prashant Mali, Luhan Yang, Kevin M Esvelt, John Aach, Marc Guell, James E DiCarlo, Julie E Norville, and George M Church. Rna-guided human genome engineering via cas9. *Science*, 339(6121):823–826, 2013.
21. Toyoaki Natsume, Tomomi Kiyomitsu, Yumiko Saga, and Masato T Kanemaki. Rapid protein depletion in human cells by auxin-inducible degron tagging with short homology donors. *Cell reports*, 15(1):210–218, 2016.
22. Leighton J Core, Joshua J Waterfall, and John T Lis. Nascent rna sequencing reveals widespread pausing and divergent initiation at human promoters. *Science*, 322(5909): 1845–1848, 2008.
23. Dig Bijay Mahat, Hojoong Kwak, Gregory T Booth, Iris H Jonkers, Charles G Danko, Ravi K Patel, Colin T Waters, Katie Munson, Leighton J Core, and John T Lis. Base-pair-resolution genome-wide mapping of active rna polymerases using precision nuclear run-on (pro-seq). *Nature protocols*, 11(8):1455, 2016.
24. Hojoong Kwak, Nicholas J Fuda, Leighton J Core, and John T Lis. Precise maps of rna polymerase reveal how promoters direct initiation and pausing. *Science*, 339(6122): 950–953, 2013.
25. Nihal Dharmasiri, Sunethra Dharmasiri, and Mark Estelle. The f-box protein tir1 is an auxin receptor. *Nature*, 435(7041):441, 2005.
26. Stefan Kepinski and Ottoline Leyser. The arabidopsis f-box protein tir1 is an auxin receptor. *Nature*, 435(7041):446, 2005.
27. Xu Tan, Luz Irina A Calderon-Villalobos, Michal Sharon, Changxue Zheng, Carol V Robinson, Mark Estelle, and Ning Zheng. Mechanism of auxin perception by the tir1 ubiquitin ligase. *Nature*, 446(7136):640, 2007.
28. Elisabeth J Chapman and Mark Estelle. Mechanism of auxin-regulated gene expression in plants. *Annual review of genetics*, 43:265–285, 2009.
29. ChenJia Shen, SuiKang Wang, YouHuang Bai, YunRong Wu, SaiNa Zhang, Ming Chen, Tom J Guilfoyle, Ping Wu, and YanHua Qi. Functional analysis of the structural domain of arf proteins in rice (oryza sativa l.). *Journal of experimental botany*, 61(14):3971–3981, 2010.
30. Dekai Wang, Kemei Pei, Yaping Fu, Zongxiu Sun, Sujuan Li, Heqin Liu, Kan Tang, Bin Han, and Yuezhi Tao. Genome-wide analysis of the auxin response factors (arf) gene family in rice (oryza sativa). *Gene*, 394(1):13–24, 2007.
31. Max H Nanao, Thomas Vinos-Poyo, Géraldine Brunoud, Emmanuel Thévenon, Meryl Mazzoleni, David Mast, Stéphanie Lainé, Shucai Wang, Gretchen Hagen, Hanbing Li, et al. Structural basis for oligomerization of auxin transcriptional regulators. *Nature communications*, 5:3617, 2014.
32. David A Korasick, Corey S Westfall, Soon Goo Lee, Max H Nanao, Renaud Dumas, Gretchen Hagen, Thomas J Guilfoyle, Joseph M Jez, and Lucia C Strader. Molecular basis for auxin response factor protein interaction and the control of auxin response repression. *Proceedings of the National Academy of Sciences*, 111(14):5427–5432, 2014.
33. Sara El-Gebali, Jaina Mistry, Alex Bateman, Sean R Eddy, Aurélien Luciani, Simon C Potter, Matloob Qureshi, Lorna J Richardson, Gustavo A Salazar, Alfredo Smart, et al. The pfam protein families database in 2019. *Nucleic Acids Research*, 47(D1):D427–D432, 2018.
34. Gavin E Crooks, Gary Hon, John-Marc Chandonia, and Steven E Brenner. Weblogo: a sequence logo generator. *Genome research*, 14(6):1188–1190, 2004.
35. Andrew Waterhouse, Martino Bertoni, Stefan Bienert, Gabriel Studer, Gerardo Tauriello, Rafal Gumienny, Florian T Heer, Tjaart A P de Beer, Christine Rempfer, Lorenza Bordoli, et al. Swiss-model: homology modelling of protein structures and complexes. *Nucleic acids research*, 2018.
36. Catherine Schuster, Evelyne Myslinski, Alain Krol, and Philippe Carbon. Staf, a novel zinc finger protein that activates the rna polymerase iii promoter of the selenocysteine trna gene. *The EMBO journal*, 14(15):3777–3787, 1995.
37. ENCODE Project Consortium et al. An integrated encyclopedia of dna elements in the human genome. *Nature*, 489(7414):57, 2012.
38. Jason S Carroll, Clifford A Meyer, Jun Song, Wei Li, Timothy R Geistlinger, Jérôme Eeckhoute, Alexander S Brodsky, Erika Krasnickas Keeton, Kirsten C Fertuck, Giles F Hall, et al. Genome-wide analysis of estrogen receptor binding sites. *Nature genetics*, 38(11): 1289, 2006.
39. Fabiana M Duarte, Nicholas J Fuda, Dig B Mahat, Leighton J Core, Michael J Guertin, and John T Lis. Transcription factors gaf and hsf act at distinct regulatory steps to modulate stress-induced gene activation. *Genes & development*, 2016.
40. Michael J Guertin, Xuesen Zhang, Scott A Coonrod, and Gordon L Hager. Transient er binding and p300 redistribution support a squelching mechanism for e2-repressed genes. *Molecular Endocrinology*, 2014.
41. Timothy E Reddy, Florencia Pauli, Rebekka O Sprouse, Norma F Neff, Kimberly M Newberry, Michael J Garabedian, and Richard M Myers. Genomic determination of the glucocorticoid response reveals unexpected mechanisms of gene regulation. *Genome research*, 2009.
42. Søren Fisker Schmidt, Bjørk Ditlev Larsen, Anne Loft, Ronni Nielsen, Jesper Grud Skat Madsen, and Susanne Mandrup. Acute tnf-induced repression of cell identity genes is mediated by nfκb-directed redistribution of cofactors from super-enhancers. *Genome research*, pages gr–188300, 2015.
43. Søren Fisker Schmidt, Bjørk Ditlev Larsen, Anne Loft, and Susanne Mandrup. Cofactor squelching: Artifact or fact? *Bioessays*, 38(7):618–626, 2016.
44. Sonia E Step, Hee-Woong Lim, Jill M Marinis, Andreas Prokesch, David J Steger, Seo-Hee You, Kyoung-Jae Won, and Mitchell A Lazar. Anti-diabetic rosiglitazone remodels the adipocyte transcriptome by redistributing transcription to pparγ-driven enhancers. *Genes & development*, 28(9):1018–1028, 2014.
45. Christopher M Vockley, Anthony M D?Ippolito, Ian C McDowell, William H Majoros, Alexias Safi, Lingyun Song, Gregory E Crawford, and Timothy E Reddy. Direct gr binding sites potentiate clusters of tf binding across the human genome. *Cell*, 166(5):1269–1281, 2016.
46. Tae-Kyung Kim, Martin Hemberg, Jesse M Gray, Allen M Costa, Daniel M Bear, Jing Wu, David A Harmin, Mike Laptewicz, Kellie Barbara-Haley, Scott Kuersten, et al. Widespread transcription at neuronal activity-regulated enhancers. *Nature*, 465(7295):182, 2010.
47. Nasun Hah, Shino Murakami, Anusha Nagari, Charles G Danko, and W Lee Kraus. Enhancer transcripts mark active estrogen receptor binding sites. *Genome research*, 2013.
48. Leighton J Core, André L Martins, Charles G Danko, Colin T Waters, Adam Siepel, and John T Lis. Analysis of nascent rna identifies a unified architecture of initiation regions at mammalian promoters and enhancers. *Nature genetics*, 46(12):1311, 2014.
49. Zhong Wang, Tinyi Chu, Lauren A Choate, and Charles G Danko. Identification of regula-

tory elements from nascent transcription using dreg. *Genome research*, 29(2):293–303, 2019.
50. Timothy L Bailey, Mikael Boden, Fabian A Buske, Martin Frith, Charles E Grant, Luca Clementi, Jingyuan Ren, Wilfred W Li, and William S Noble. Meme suite: tools for motif discovery and searching. *Nucleic acids research*, page gkp335, 2009.
51. Maxim V Kuleshov, Matthew R Jones, Andrew D Rouillard, Nicolas F Fernandez, Qiaonan Duan, Zichen Wang, Simon Koplev, Sherry L Jenkins, Kathleen M Jagodnik, Alexander Lachmann, et al. Enrichr: a comprehensive gene set enrichment analysis web server 2016 update. *Nucleic acids research*, 44(W1):W90–W97, 2016.
52. Raymond Lo and Jason Matthews. High-resolution genome-wide mapping of ahr and arnt binding sites by chip-seq. *Toxicological sciences*, 130(2):349–361, 2012.
53. Nicholas J Fuda, M Behfar Ardehali, and John T Lis. Defining mechanisms that regulate rna polymerase ii transcription in vivo. *Nature*, 461(7261):186, 2009.
54. Clarissa Scholes, Angela H DePace, and Álvaro Sánchez. Combinatorial gene regulation through kinetic control of the transcription cycle. *Cell systems*, 4(1):97–108, 2017.
55. Karen Adelman, Wenxiang Wei, M Behfar Ardehali, Janis Werner, Bing Zhu, Danny Reinberg, and John T Lis. Drosophila paf1 modulates chromatin structure at actively transcribed genes. *Molecular and cellular biology*, 26(1):250–260, 2006.
56. Michael J Guertin and John T Lis. Chromatin landscape dictates hsf binding to target dna elements. *PLoS genetics*, 6(9):e1001114, 2010.
57. Stephanie A Morris, Songjoon Baek, Myong-Hee Sung, Sam John, Malgorzata Wiench, Thomas A Johnson, R Louis Schiltz, and Gordon L Hager. Overlapping chromatin-remodeling systems collaborate genome wide at dynamic chromatin transitions. *Nature structural & molecular biology*, 21(1):73, 2014.
58. Laurie A Stargell and Kevin Struhl. Mechanisms of transcriptional activation in vivo: two steps forward. *Trends in Genetics*, 12(8):311–315, 1996.
59. Hiroshi Sakurai and Toshio Fukasawa. Functional connections between mediator components and general transcription factors of saccharomyces cerevisiae. *Journal of Biological Chemistry*, 275(47):37251–37256, 2000.
60. Cyril Esnault, Yad Ghavi-Helm, Sylvain Brun, Julie Soutourina, Nynke Van Berkum, Claire Boschiero, Frank Holstege, and Michel Werner. Mediator-dependent recruitment of tfiih modules in preinitiation complex. *Molecular cell*, 31(3):337–346, 2008.
61. Chhabi K Govind, Sungpil Yoon, Hongfang Qiu, Sudha Govind, and Alan G Hinnebusch. Simultaneous recruitment of coactivators by gcn4p stimulates multiple steps of transcription in vivo. *Molecular and cellular biology*, 25(13):5626–5638, 2005.
62. NICHOLAS F Marshall and DAVID H Price. Control of formation of two distinct classes of rna polymerase ii elongation complexes. *Molecular and cellular biology*, 12(5):2078–2090, 1992.
63. Karen Adelman and John T Lis. Promoter-proximal pausing of rna polymerase ii: emerging roles in metazoans. *Nature Reviews Genetics*, 13(10):720, 2012.
64. M Behfar Ardehali, Jie Yao, Karen Adelman, Nicholas J Fuda, Steven J Petesch, Watt W Webb, and John T Lis. Spt6 enhances the elongation rate of rna polymerase ii in vivo. *The EMBO journal*, 28(8):1067–1077, 2009.
65. Tom J Guilfoyle and Gretchen Hagen. Auxin response factors. *Current opinion in plant biology*, 10(5):453–460, 2007.
66. Luz Irina A Calderón Villalobos, Sarah Lee, Cesar De Oliveira, Anthony Ivetac, Wolfgang Brandt, Lynne Armitage, Laura B Sheard, Xu Tan, Geraint Parry, Haibin Mao, et al. A combinatorial tir1/afb–aux/iaa co-receptor system for differential sensing of auxin. *Nature chemical biology*, 8(5):477, 2012.
67. Richard Patryk Ngondo-Mbongo, Evelyne Myslinski, Jon C Aster, and Philippe Carbon. Modulation of gene expression via overlapping binding sites exerted by znf143, notch1 and thap11. *Nucleic acids research*, 41(7):4000–4014, 2013.
68. Swneke D Bailey, Xiaoyang Zhang, Kinjal Desai, Malika Aid, Olivia Corradin, Richard Cowper-Sal, Batool Akhtar-Zaidi, Peter C Scacheri, Benjamin Haibe-Kains, Mathieu Lupien, et al. Znf143 provides sequence specificity to secure chromatin interactions at gene promoters. *Nature communications*, 6:6186, 2015.
69. Yad Ghavi-Helm, Felix A Klein, Tibor Pakozdi, Lucia Ciglar, Daan Noordermeer, Wolfgang Huber, and Eileen EM Furlong. Enhancer loops appear stable during development and are associated with paused polymerase. *Nature*, 512(7512):96, 2014.
70. Kara L McKinley and Iain M Cheeseman. Large-scale analysis of crispr/cas9 cell-cycle knockouts reveals the diversity of p53-dependent responses to cell-cycle defects. *Developmental cell*, 40(4):405–420, 2017.
71. F Ann Ran, Patrick D Hsu, Jason Wright, Vineeta Agarwala, David A Scott, and Feng Zhang. Genome engineering using the crispr-cas9 system. *Nature protocols*, 8(11):2281, 2013.
72. Qiupeng Zheng, Xiaohong Cai, Meng How Tan, Steven Schaffert, Christopher P Arnold, Xue Gong, Chang-Zheng Chen, and Shenglin Huang. Precise gene deletion and replacement using the crispr/cas9 system in human cells. *Biotechniques*, 57(3):115–124, 2014.
73. Harvey Motulsky and Arthur Christopoulos. *Fitting models to biological data using linear and nonlinear regression: a practical guide to curve fitting.* Oxford University Press, 2004.
74. Marcel Martin. Cutadapt removes adapter sequences from high-throughput sequencing reads. *EMBnet. journal*, 17(1):pp–10, 2011.
75. André L Martins and Michael J. Guertin. Remove pcr duplicates from fastq files. *https://github.com/guertinlab/fqdedup*, 2018.
76. Assaf Gordon. Fastx toolkit. *https://github.com/agordon/fastx_toolkit*, 2010.
77. Ben Langmead, Cole Trapnell, Mihai Pop, and Steven Salzberg. Ultrafast and memory-efficient alignment of short dna sequences to the human genome. *Genome Biology*, 10(3): R25, 2009. ISSN 1465-6906. doi: 10.1186/gb-2009-10-3-r25.
78. Heng Li, Bob Handsaker, Alec Wysoker, Tim Fennell, Jue Ruan, Nils Homer, Gabor Marth, Goncalo Abecasis, Richard Durbin, et al. The sequence alignment/map format and samtools. *Bioinformatics*, 25(16):2078–2079, 2009.
79. André L Martins, Ninad M Walavalkar, Warren D Anderson, Chongzhi Zang, and Michael J Guertin. Universal correction of enzymatic sequence bias reveals molecular signatures of protein/dna interactions. *Nucleic acids research*, 46(2):e9–e9, 2017.
80. André L Martins. R interface to query ucsc bigwig files. *https://github.com/andrelmartins/bigWig*, 2014.
81. W James Kent, Ann S Zweig, G Barber, Angie S Hinrichs, and Donna Karolchik. Bigwig and bigbed: enabling browsing of large distributed datasets. *Bioinformatics*, 26(17): 2204–2207, 2010.
82. Aaron R Quinlan and Ira M Hall. Bedtools: a flexible suite of utilities for comparing genomic features. *Bioinformatics*, 26(6):841–842, 2010.
83. Michael I Love, Wolfgang Huber, and Simon Anders. Moderated estimation of fold change and dispersion for rna-seq data with deseq2. *bioRxiv*, 2014.
84. Timothy L Bailey, James Johnson, Charles E Grant, and William S Noble. The meme suite. *Nucleic acids research*, 43(W1):W39–W49, 2015.
85. Sven Heinz, Christopher Benner, Nathanael Spann, Eric Bertolino, Yin C Lin, Peter Laslo, Jason X Cheng, Cornelis Murre, Harinder Singh, and Christopher K Glass. Simple combinations of lineage-determining transcription factors prime cis-regulatory elements required for macrophage and b cell identities. *Molecular cell*, 38(4):576–589, 2010.

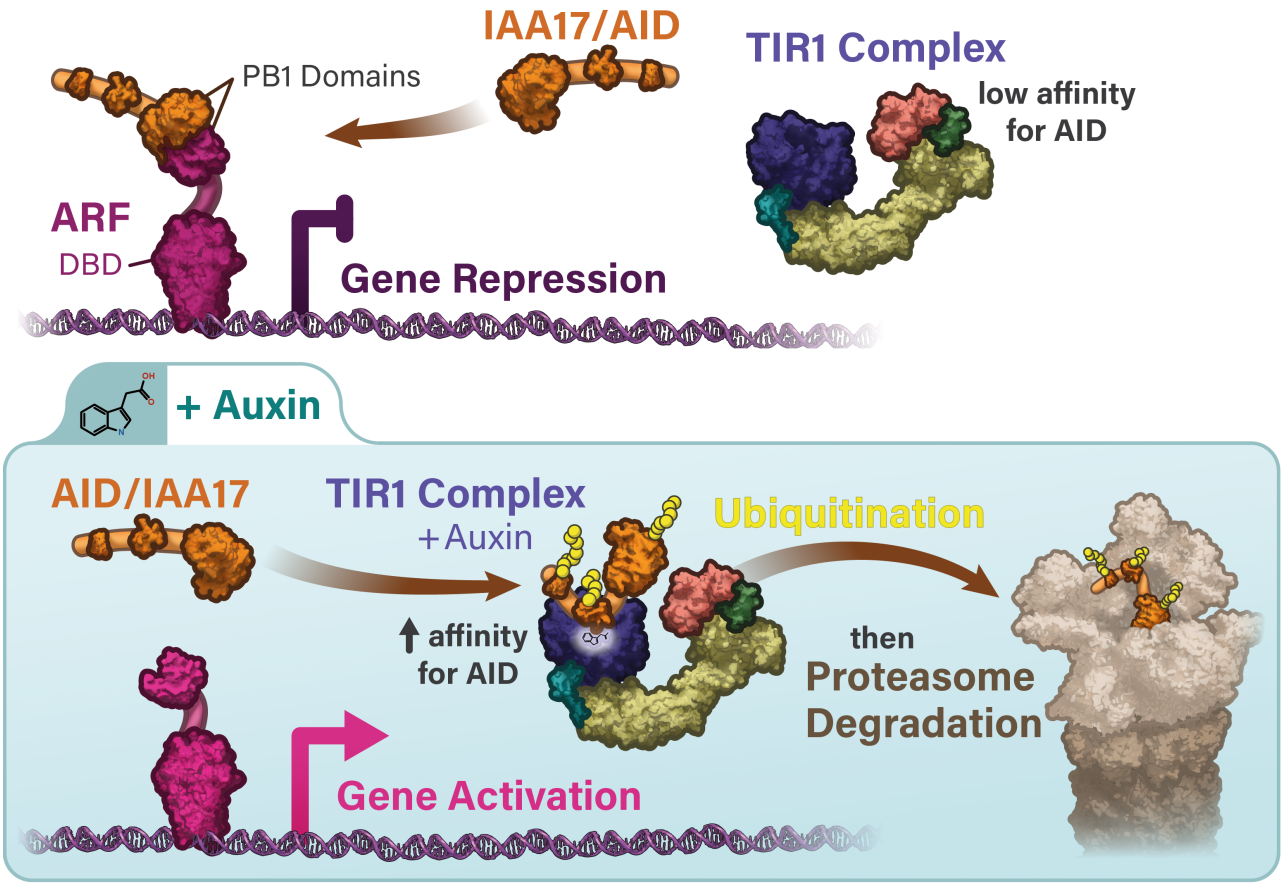

Fig. S1. ARF is critical for the proper regulation of the auxin-induced transcriptional response in plants. In the absence of auxin, IAA binds the PB1 domain of ARF. Auxin binds to TIR1 and drives strong association of TIR1 with IAA to mediate ubiquitination and degradation.

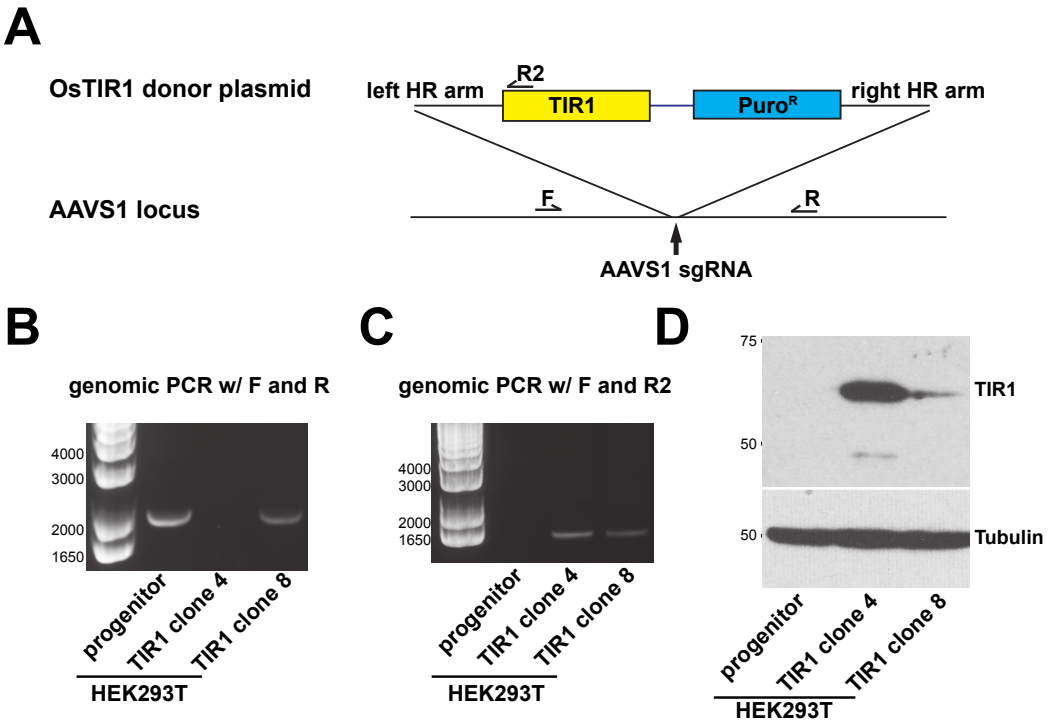

Fig. S2. TIR1 was integrated into the AAVS1 locus of HEK293T cells. A) A schematic of the strategy to integrate CMV-driven TIR1 into the AAVS1 locus of the HEK293T cells using the CRISPR-Cas9 system. Primers F and R2 generate an amplicon if the construct is inserted. F and R primers flank the insert and will amplify if the construct does not insert into a copy of AAVS1. B) At least one copy of AAVS1 contains the insertion in both clone 4 and clone 8. C) All copies of AAVS1 contain the insertion in clone 4, but clone 8 is heterozygous. D) Western blotting indicates that the TIR1 protein is expressed in both clones.

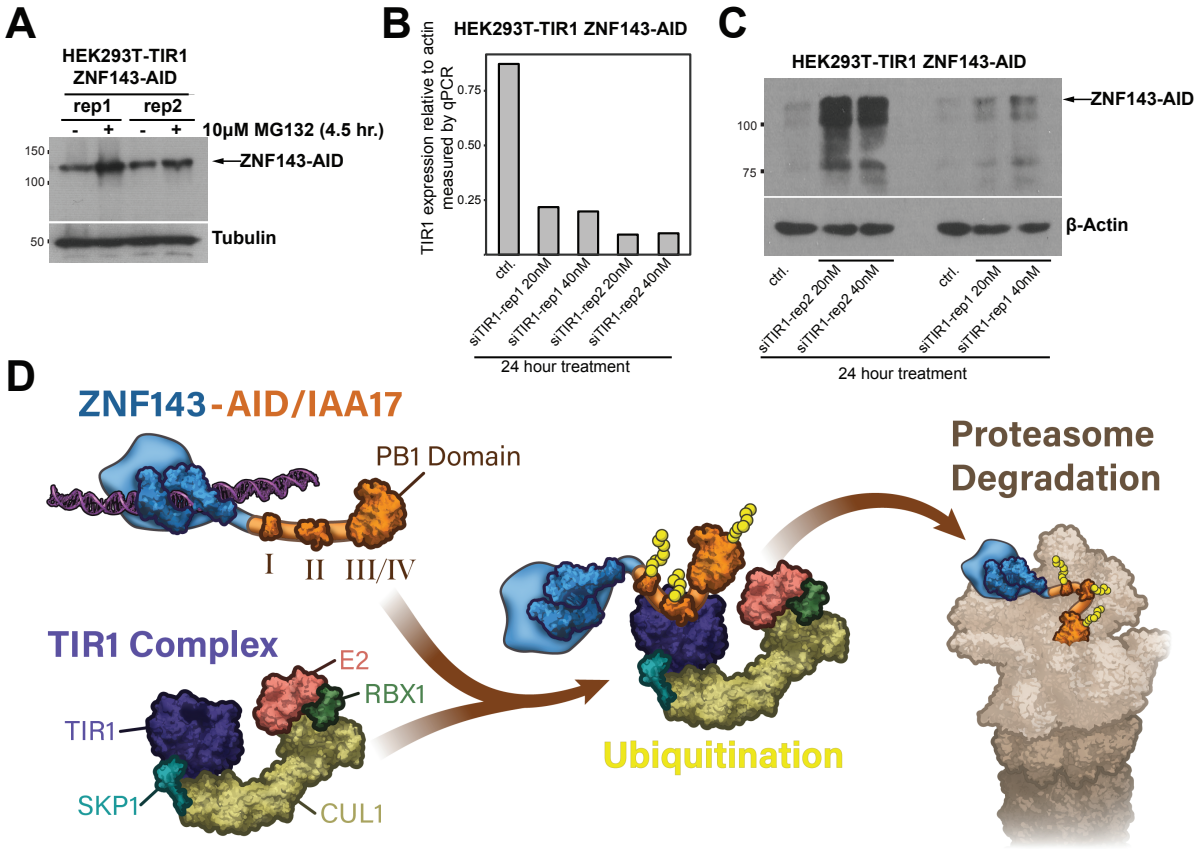

Fig. S3. Chronic auxin-independent depletion is proteasome dependent. A) Two independent clones (rep1 and rep2) of ZNF143-AID tagged cells were treated with MG132 for four hours. ZNF143 protein levels increase after MG132 treatment. B) TIR1 was depleted to between 10% and 20% of the control levels as measured by qPCR. C) TIR1 depletion stabilizes ZNF143-AID and stabilization correlates with the degree of the TIR1 knockdown. D) An auxin-independent interaction between ZNF143-AID and TIR1 is proposed to drive chronic proteosomal degradation.

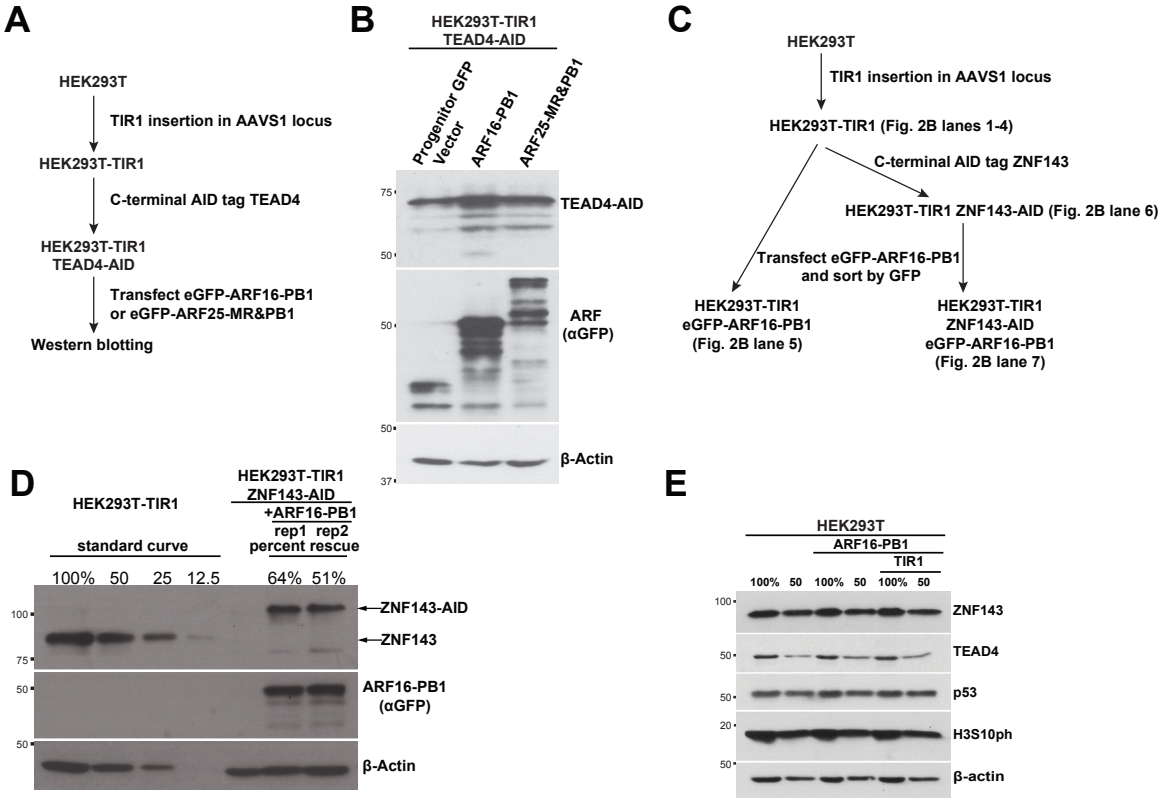

Fig. S4. Expression of the ARF domains rescues chronic protein depletion, but does not detectably affect protein levels in the absence of AID-tagging. A) A schematic of the strategy to express ARF (PB1 domain of ARF16 or the MR and PB1 domain of ARF25) within HEK293T cells that express TIR1 and AID-tagged TEAD4. B) TEAD4-AID protein is stabilized after expression GFP-ARF16-PB1 and GFP-ARF25-MR-PB1, but not stabilized by the empty vector that expresses GFP. C) The illustrated workflow highlights the source of each lane in Figure 2B. D) Expression of the ARF16 PB1 domain rescues ZNF143 levels to 51% to 64% the level of untagged ZNF143. E) ARF16-PB1 and TIR1 expression had no effect on the expression of ZNF143, TEAD4, and p53; actin and phosphorylated H3S10 are loading controls.

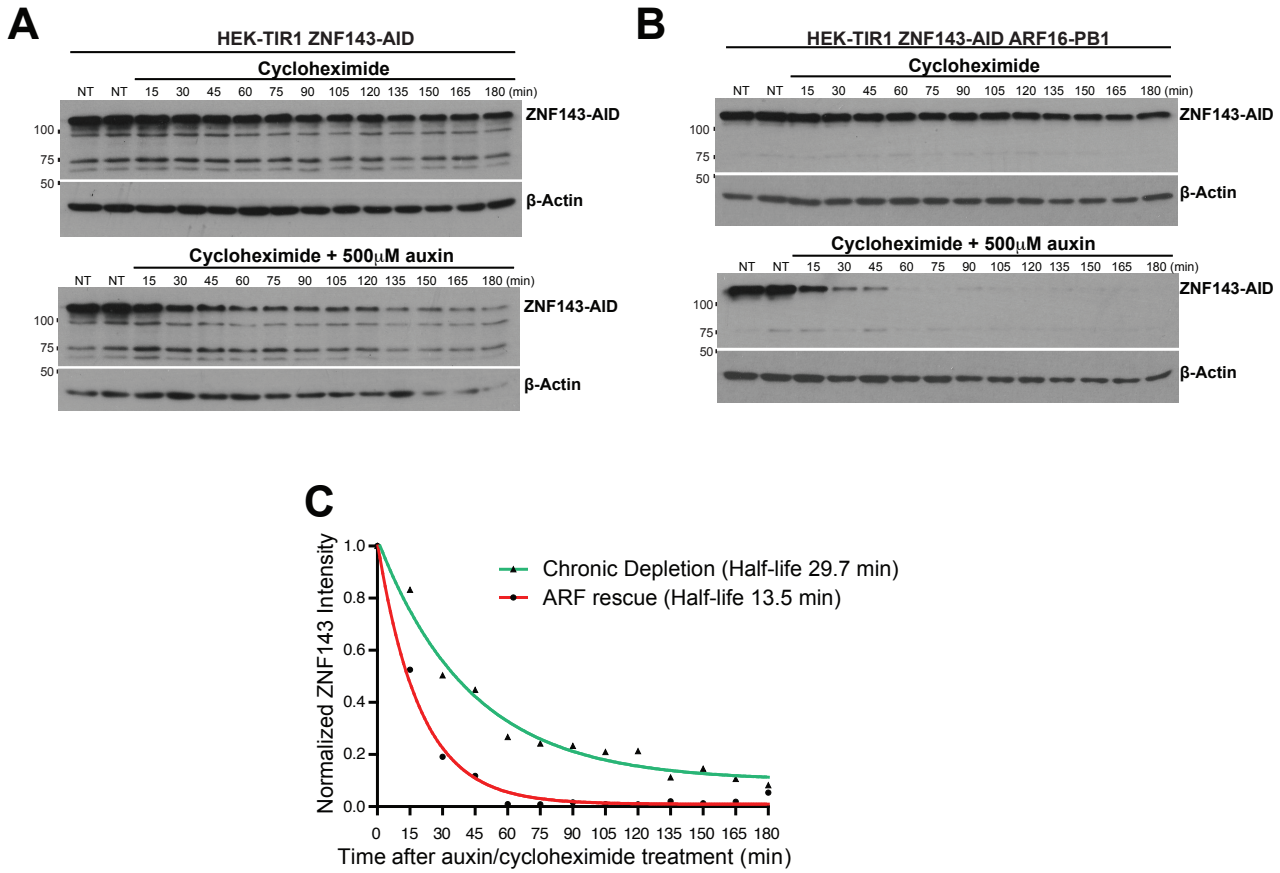

Fig. S5. ARF rescue increases the rate of auxin dependent degradation of AID tagged protein. HEK293T-TIR1 ZNF143-AID cells (A) and ARF-16-rescued cells (B) were treated with cycloheximide alone, or cycloheximide in combination with auxin, to compare degradation kinetics upon inhibiting translation. C) Densitometric quantification measurements of ZNF143-AID bands from the lower blots in panel A (green trace) and panel B (red trace) were plotted and fit to a one phase decay equation.

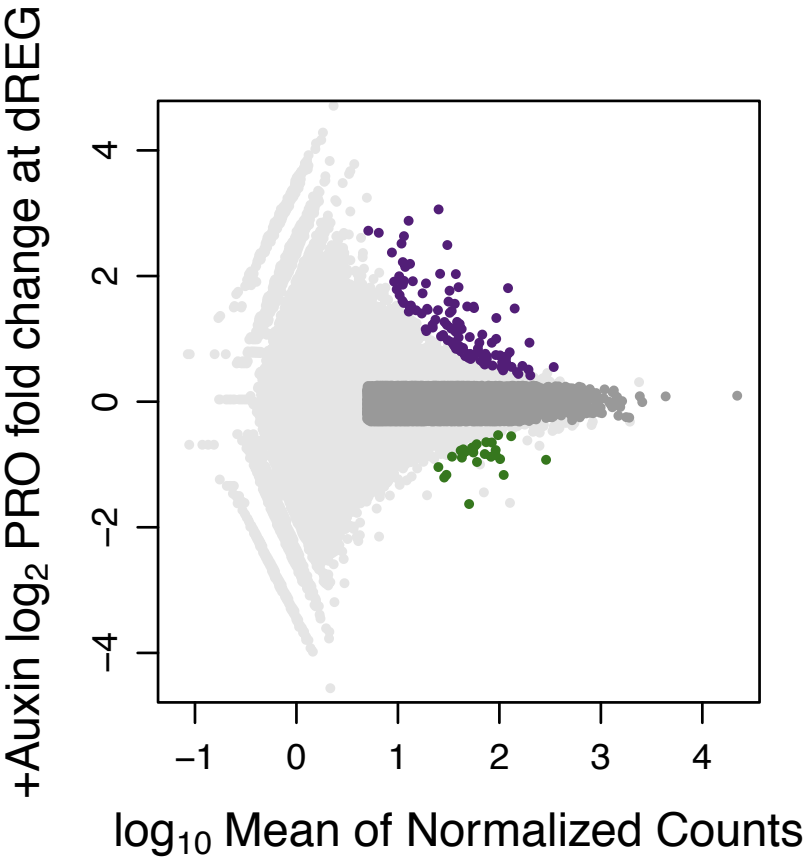

Fig. S6. Bidirectional transcription changes modestly at a subset of dREG-defined (49) regulatory elements upon ZNF143 depletion.

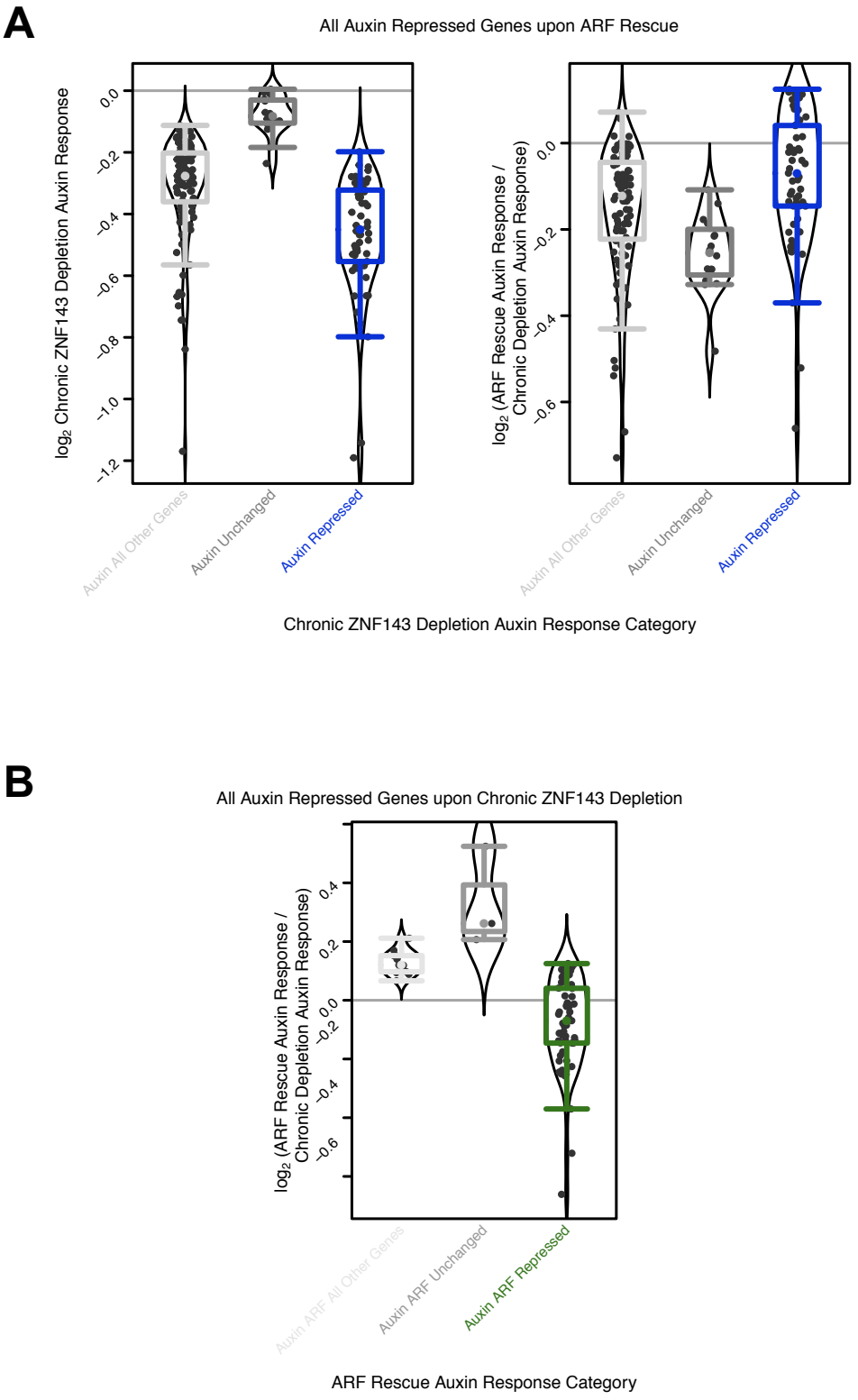

Fig. S7. ZNF143-repressed genes decrease expression in the chronic depletion background, but below our sensitivity of detection. A) Despite falling in *unchanged* and *all other genes* classes, the net response upon auxin treatment in the chronic depletion background is consistent in direction with auxin response in the rescue. Genes have a greater magnitude of response in the rescue compared to chronic depletion. B) Repressed genes in the chronic depletion background are not consistently auxin-repressed and we do not consistently observe a greater magnitude of auxin-response in the ARF-rescue. These data suggest that the changes in gene expression in the chronic depletion background may not be ZNF143-specific.

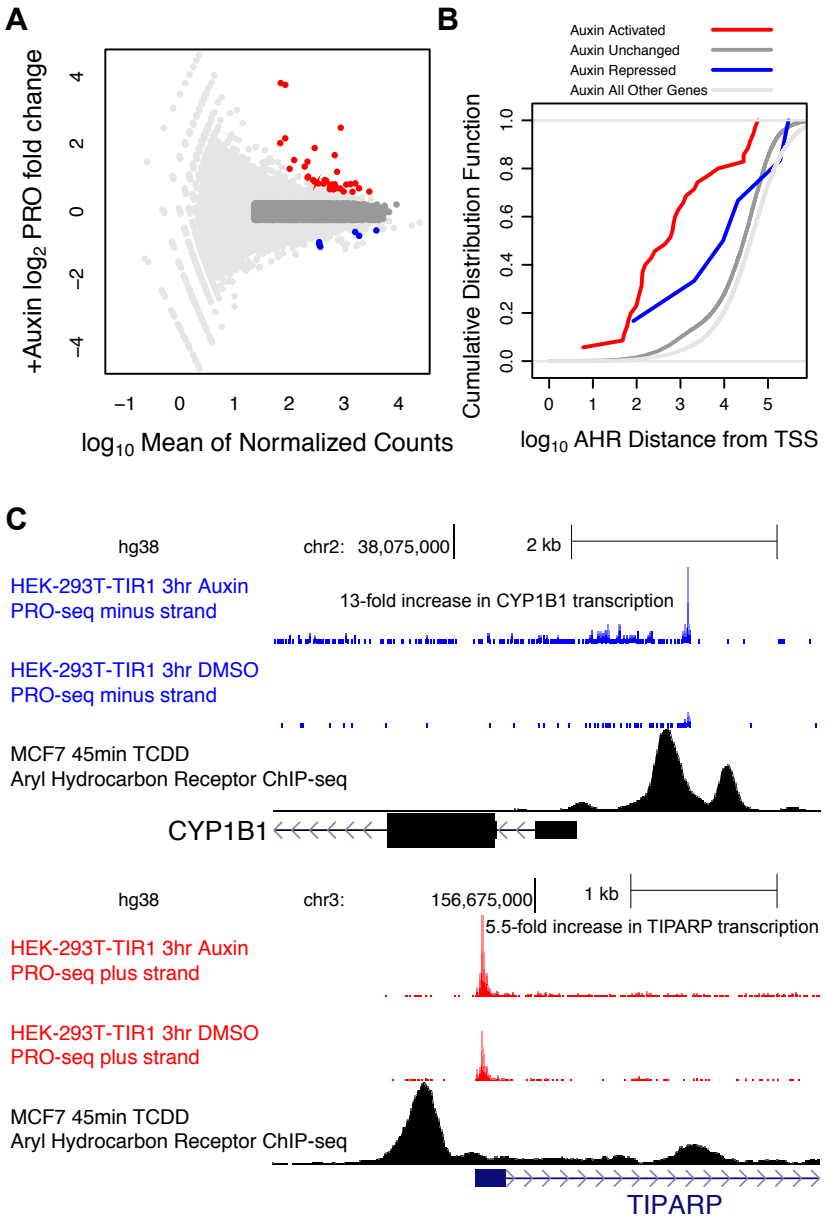

Fig. S8. Auxin treatment activates Aryl Hydrocarbon Receptor (AHR) gene targets. A) Auxin treatment activates many genes compared to a DMSO control treatment. B) Auxin-activated genes are, on average, closer to AHR binding sites. C) The genes TIPARP and CYP1B1 are examples of canonical hydrocarbon-responsive genes, both of which are activated by auxin and bound by AHR. Note that the transcription start site for CYP1B1 is upstream of the gene annotation in HEK293T cells.

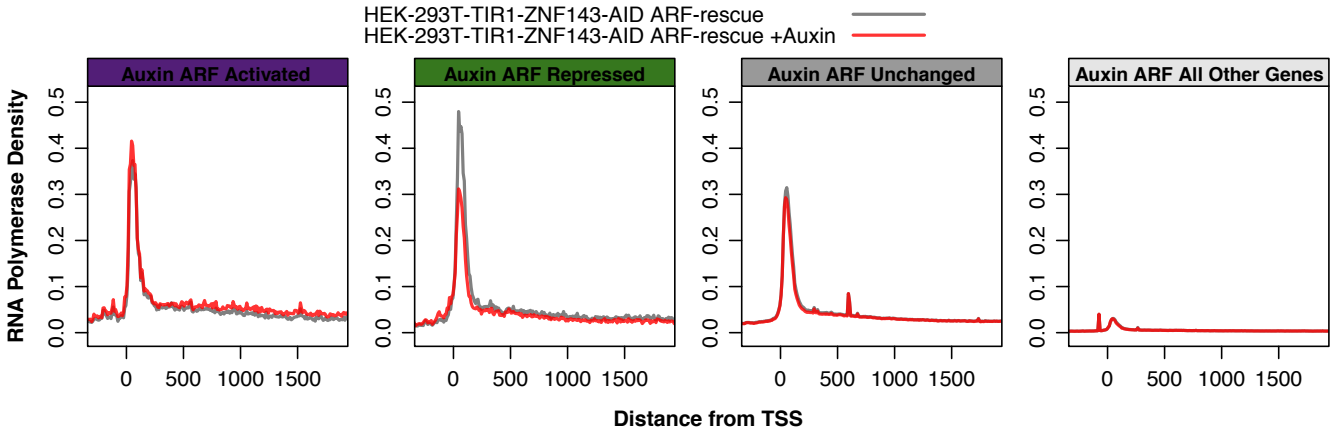

Fig. S9. Average RNA Polymerase occupancy plots, or composite profiles, suggest that RNA Polymerase pause density is reduced in the repressed gene class with only modest differences in the other classes.

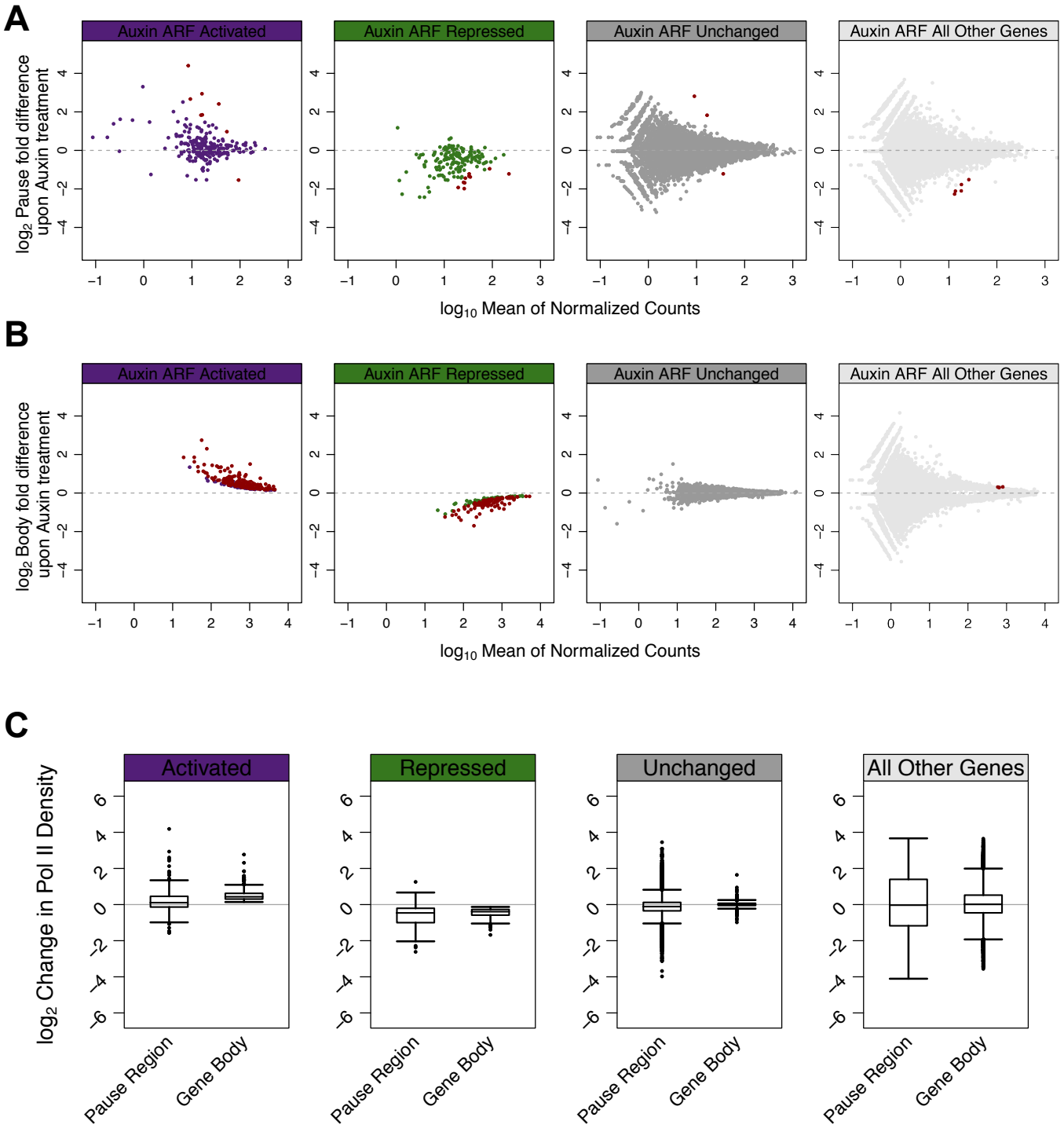

Fig. S10. Individual gene analysis indicates RNA Polymerase pause density is reduced in the pause and gene body. A) Pol II pausing is consistently decreased in the auxin-repressed class. Red genes fall below an FDR threshold of 0.01. B) Each panel's gene class was previously defined by the changes that occur over the entire gene length, which is dominated by the gene body; therefore, red genes (FDR threshold of 0.0001) are consistent with their classification. Note that the x-axis for panels A and B are not identical and only a few genes have a $\log_{10}$ mean count above 2 in the pause region for the repressed class, compared to only a few genes below a $\log_{10}$ mean count of 2 in the gene body. C) Box and whisker plots collapse the data from panels A&B above.

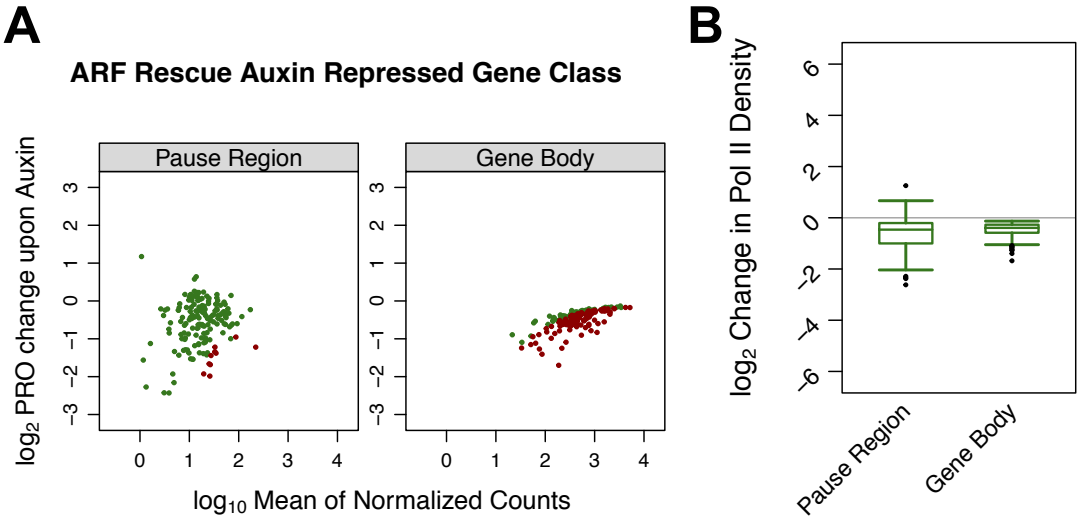

Fig. S11. RNA Polymerase pause density is reduced in the pause region and gene body at genes that are repressed upon ZNF143 depletion. The gene body and pause region data for the repressed class from Figure S10 are shown side-by-side.

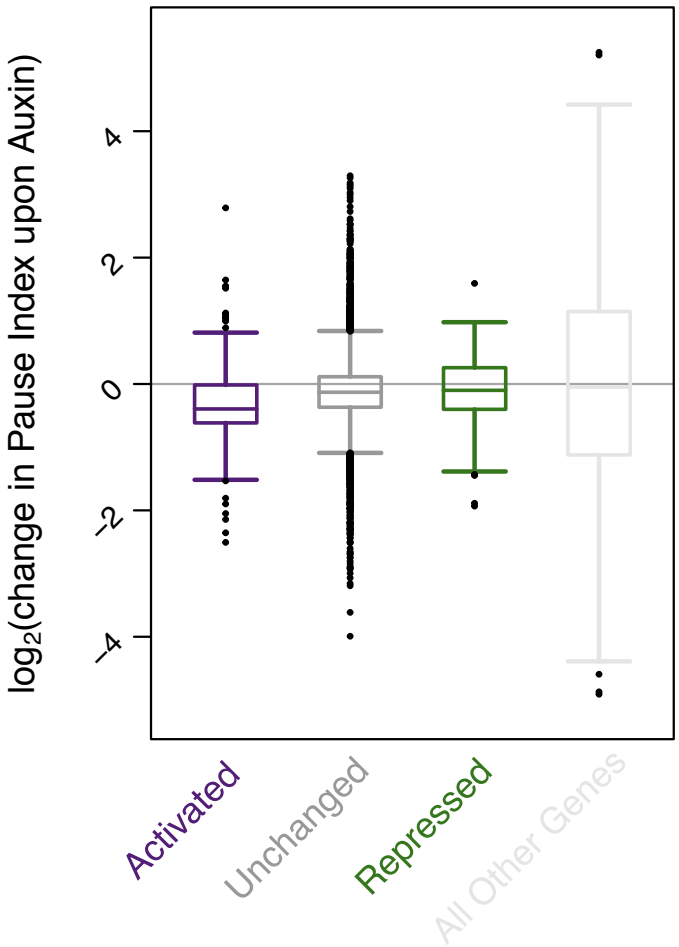

Fig. S12. The pause index changes only modestly ($\log_2$ values of approximately 0) for repressed genes. A modest average decrease in pause index is also observed for the control (unchanged) gene class.